



HAL
open science

Efficient Recovery of Rare Earth Elements (Pr(III) and Tm(III)) From Mining Residues Using a New Phosphorylated Hydrogel (Algal Biomass/PEI)

Chunlin He, Khalid A.M. Salih, Yuezhou Wei, Hamed Mira, Adel A-H Abdel-Rahman, Khalid Z. Elwakeel, Mohammed F Hamza, Guibal Eric

► To cite this version:

Chunlin He, Khalid A.M. Salih, Yuezhou Wei, Hamed Mira, Adel A-H Abdel-Rahman, et al.. Efficient Recovery of Rare Earth Elements (Pr(III) and Tm(III)) From Mining Residues Using a New Phosphorylated Hydrogel (Algal Biomass/PEI). *Metals*, 2021, Leaching/Bioleaching and Recovery of Metals, 11 (2), pp.294. 10.3390/met11020294 . hal-03135905

HAL Id: hal-03135905

<https://imt-mines-ales.hal.science/hal-03135905>

Submitted on 12 Feb 2021

HAL is a multi-disciplinary open access archive for the deposit and dissemination of scientific research documents, whether they are published or not. The documents may come from teaching and research institutions in France or abroad, or from public or private research centers.

L'archive ouverte pluridisciplinaire **HAL**, est destinée au dépôt et à la diffusion de documents scientifiques de niveau recherche, publiés ou non, émanant des établissements d'enseignement et de recherche français ou étrangers, des laboratoires publics ou privés.

Article

Efficient Recovery of Rare Earth Elements (Pr(III) and Tm(III)) From Mining Residues Using a New Phosphorylated Hydrogel (Algal Biomass/PEI)

Chunlin He ¹, Khalid A.M. Salih ¹, Yuezhou Wei ^{1,2}, Hamed Mira ³, Adel A.-H. Abdel-Rahman ⁴, Khalid Z. Elwakeel ^{5,6}, Mohammed F. Hamza ^{1,3,*} and Eric Guibal ^{7,*}

- ¹ Guangxi Key Laboratory of Processing for Non-Ferrous Metals and Featured Materials, School of Resources, Environment and Materials, Guangxi University, Nanning 530004, China; helink@gxu.edu.cn (C.H.); Immortaltiger7@gmail.com (K.A.M.S.); yzwei@gxu.edu.cn (Y.W.)
- ² School of Nuclear Science and Engineering, Shanghai Jiao Tong University, Shanghai 200240, China
- ³ Nuclear Materials Authority, P.O. Box, El-Maadi, Cairo 530, Egypt; hamedmira@yahoo.com
- ⁴ Faculty of Science, Menoufia University, Shebine El-Koam 00123, Egypt; adelnassar63@yahoo.com
- ⁵ Department of Chemistry, College of Science, University of Jeddah, Jeddah 23218, Saudi Arabia; kelwkeel@uj.edu.sa
- ⁶ Environmental Science Department, Faculty of Science, Port-Said University, Port Said 42526, Egypt
- ⁷ Polymers, Composites and Hybrids, Institut Mines Telecom—Mines Ales, F-30100 Ales, France
- * Correspondence: m_fouda21@hotmail.com (M.F.H.); eric.guibal@mines-ales.fr (E.G.); Tel.: +2-01116681228 (M.F.H.); +33-(0)466782734 (E.G.)



Citation: He, C.; Salih, K.A.M.; Wei, Y.; Mira, H.; Abdel-Rahman, A.A.-H.; Elwakeel, K.Z.; Hamza, M.F.; Guibal, E. Efficient Recovery of Rare Earth Elements (Pr(III) and Tm(III)) From Mining Residues Using a New Phosphorylated Hydrogel (Algal Biomass/PEI). *Metals* **2021**, *11*, 294. <https://doi.org/10.3390/met11020294>

Academic Editor: Laura Castro
Received: 11 January 2021
Accepted: 2 February 2021
Published: 8 February 2021

Publisher's Note: MDPI stays neutral with regard to jurisdictional claims in published maps and institutional affiliations.



Copyright: © 2021 by the authors. Licensee MDPI, Basel, Switzerland. This article is an open access article distributed under the terms and conditions of the Creative Commons Attribution (CC BY) license (<https://creativecommons.org/licenses/by/4.0/>).

Abstract: With the target of recovering rare earth elements (REEs) from acidic leachates, a new functionalized hydrogel was designed, based on the phosphorylation of algal/polyethyleneimine beads. The functionalization strongly increased the sorption efficiency of the raw material for Pr(III) and Tm(III). Diverse techniques were used for characterizing this new material and correlating the sorption performances and mechanisms to the physicochemical structure of the sorbent. First, the work characterized the sorption properties from synthetic solutions with the usual procedures (study of pH effect, uptake kinetics, sorption isotherms, metal desorption and sorbent recycling, and selectivity from multi-element solutions). Optimum pH was found close to 5; sorption isotherms were fitted by the Langmuir equation (maximum sorption capacities close to 2.14 mmol Pr g⁻¹ and 1.57 mmol Tm g⁻¹). Fast uptake kinetics were modeled by the pseudo-second order rate equation. The sorbent was highly selective for REEs against alkali-earth and base metals. The sorbent was remarkably stable for sorption and desorption operation (using 0.2 M HCl/0.5 M CaCl₂ solutions). The sorbent was successfully applied to the leachates of Egyptian ore (pug leaching) after a series of pre-treatments (precipitation steps), sorption, and elution. The selective precipitation of REEs using oxalic acid allows for the recovery of a pure REE precipitate.

Keywords: rare earth elements; sorption isotherms; uptake kinetics; functionalization of bio-based sorbent; metal desorption; sorbent recycling; treatment of ore leachate

1. Introduction

Rare earth elements (REEs) are widely used in the design of high-tech devices [1]. For example, praseodymium is used for elaborating advanced alloys (aircraft industry), refractory substances, coloring materials, lighting equipment, and fiber optical cables [2]. Thulium is an expensive REE that is used for designing x-ray emitters, medical and astronomical lasers [3], high-temperature superconductors, ferrite alloys, and ceramic magnetic materials in microwave equipment. In addition to their relatively expensive costs, the geopolitical distribution of resources and exploitation facilities of these metals are making these elements strategic targets, so there is great attention toward developing recovery processes from low-grade minerals and/or from industrial wastes [4]. Their rarefaction,

cost, and weak recycling rate (less than 10% for both Tm and Pr, [5]) justify the importance of designing new processes for their recovery from low-grade resources [6].

Their recovery proceeds as sub-products from the processing of other metals from diverse resources: red mud valorization, phosphoric acid synthesis from phosphate ores [7], and ore leachates. The usual hydrometallurgical processes such as solvent extraction [8] and sorption on resins [9–11] can be applied for the treatment of high or low concentration effluents, respectively [12]. The complexity of the leachates (due to the presence of many transition metals) requires developing processes efficient for the separation of REEs from base metals [13]. Furthermore, the physicochemical properties of the members of the REE family are so close that their separation is usually very complex, requiring long chromatographic columns with many theoretical plateaus. These separation issues represent important global challenges for designing competitive processes for the selective recovery of REEs.

There has been an impressive effort, demonstrated by the numerous literature published over the last decade, in developing new sorbents bearing the same reactive groups as those active in the extractants used in solvent extraction [14–18]. Sorbents have been designed by the functionalization of clays for the recovery of REEs [19] and the preparation of composites based on silica [20–23] or carbon-based supports [21,24,25]. Synthetic resins have been functionalized with phosphorus groups [26–31], taking advantage of the affinity of phosphonic-based reactive groups for REEs.

Biosorption processes have already been reported for the recovery of REEs including algal biomass [32,33] and alginate (a polysaccharide bearing guluronic and mannuronic acid groups) [34–39]. Alginate is frequently used for metal sorption making profit of the reactivity of carboxylate groups [40,41], but also as a constituent of composite sorbents [42]. Recently, the combination of (a) specific interactions of alginate (partially extracted from algal biomass) with poly(ethyleneimine) (PEI), the ionotropic gelation of alginate with calcium chloride, and the crosslinking of amine groups (of PEI) with glutaraldehyde (GA) was used for synthesizing composite hydrogel beads (algal-polyethyleneimine beads, APEI) [43]. These supports have been functionalized by grafting amidoxime groups for Sr(II) sorption [44], sulfonic groups for the recovery of REEs [45], and by quaternization for Sc(III) removal [46]. The current work describes the synthesis of phosphorylated APEI beads (P2-APEI). The support (i.e., APEI) is activated with epichlorohydrin (APEI-Cl) (which is subject to a partial polymerization under selected experimental conditions) before being reacted with triethyl phosphine. After physicochemical characterization (using various analytical tools), the phosphonated-functionalized sorbent (i.e., P2-APEI) is extensively investigated for the sorption of Pr(III) (which is part of light REE, LREEs) and Tm(III) (representing heavy REEs, HREEs). After pH optimization, the uptake kinetics and sorption isotherms are investigated using conventional models for fitting experimental profiles. The selectivity properties are investigated against transition metals at different pH values to evaluate the possibility to separate base metals from REEs, but also to discuss the possibility of separating the rare earths (LREEs vs. HREEs). The elution of REEs is investigated and applied for five cycles of sorption and desorption for evaluating the potential of the sorbent to be re-used. In the last section of this work, the sorbent is tested for the recovery and separation of REEs from the acidic leachates of waste residue of Egyptian ore. This section includes the study of the pre-treatment of leachates, the sorption process, the elution of the loaded sorbent, and the final precipitation of REEs as oxalate salt.

2. Materials and Methods

2.1. Materials

Brown algae (*Laminaria digitata*) was provided by Setalg (Pleubian, France). After washing, drying, and grinding, the biomass was sieved to recover the fraction below 250 μm . Alginate (Manugel GMB) was supplied by DuPont (Landerneau, France; now JRS Rettenmaier). Other reagents such as sodium carbonate Na_2CO_3 (99.8%) and calcium chloride (96%) were purchased from Chem-Lab NV (Zedelgem, Belgium). Branched

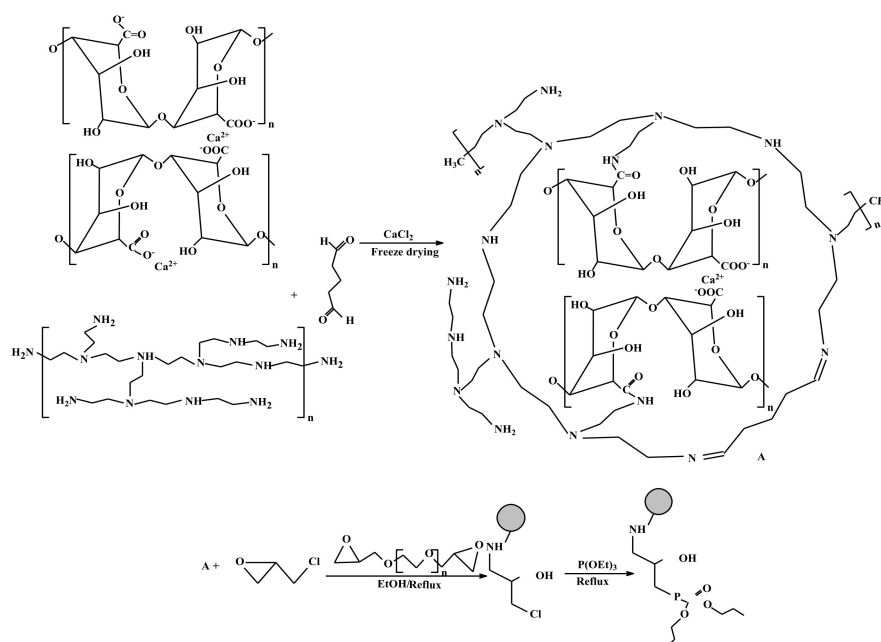
polyethyleneimine (bPEI, 50% (*w/w*) in water) and glutaraldehyde (GA, 50% (*w/w*) in water) were purchased from Sigma-Aldrich (Taufkirchen, Germany).

Epichlorohydrin (98%) and triethyl phosphite (98%) were purchased from Shanghai Maklin Biochemical Co. Ltd. (Shanghai, China). Zinc oxide (98%) (for selectivity exp.) was supplied by Aladdin Industrial Corporation (Shanghai, China). Aluminum sulfate octadecahydrate (99%) (used in selectivity experiments), sodium hydroxide (96%), and absolute ethanol (99.7%) were supplied by Guangdong Guanghua Sci-Tech (Guangzhou, China). Acetone (95.5%) and sulfuric acid (98%) were purchased from Chron Chemicals (Sichuan Province, China). Praseodymium sulfate (99.99%) and thulium sulfate (99.99%) were supplied by National Engineering Research Center of Rare Earth Metallurgy and Functional Materials Co. Ltd. (Baotou city, Inner Mongolia, China). Silicon with conc. (1000 ppm) as a source of Si, which was supplied by Guobiao Inspection and Certification Co. Ltd. (Huairou District, Beijing, China). The other reagents were Prolabo products and were used as received.

2.2. Synthesis of Sorbents

2.2.1. Synthesis of Algal/Poly(ethyleneimine) (PEI) Beads (APEI)

The algal/PEI beads were prepared according to a method previously described by Wang et al. [43]. Briefly, 18.75 g of dry algal biomass was dispersed into 750 mL of Na_2CO_3 solution (1%, *w/w*) under agitation and heating (50 °C) for 24 h. After cooling, a volume (i.e., 250 mL) of alginate solution (4%, *w/w*) was added to biomass suspension. A volume of 5 mL of bPEI solution (50%, *w/w*) was added to 500 mL of the mixture under agitation. The algal biomass/alginate/ bPEI suspension was distributed into a 1-L volume of a solution containing both CaCl_2 (1%, *w/w*) and GA (5 mL, 50%, *w/w*). The beads (APEI) were maintained under agitation overnight in the crosslinking solution before being filtrated and freeze-dried. The size of the APEI beads was 2.9 ± 0.2 mm. The successive steps in the functionalization of APEI beads are reported in Scheme 1.



Scheme 1. Synthesis pathway for the synthesis of P2-APEI sorbent (A: poly(ethyleneimine) (APEI) synthesis).

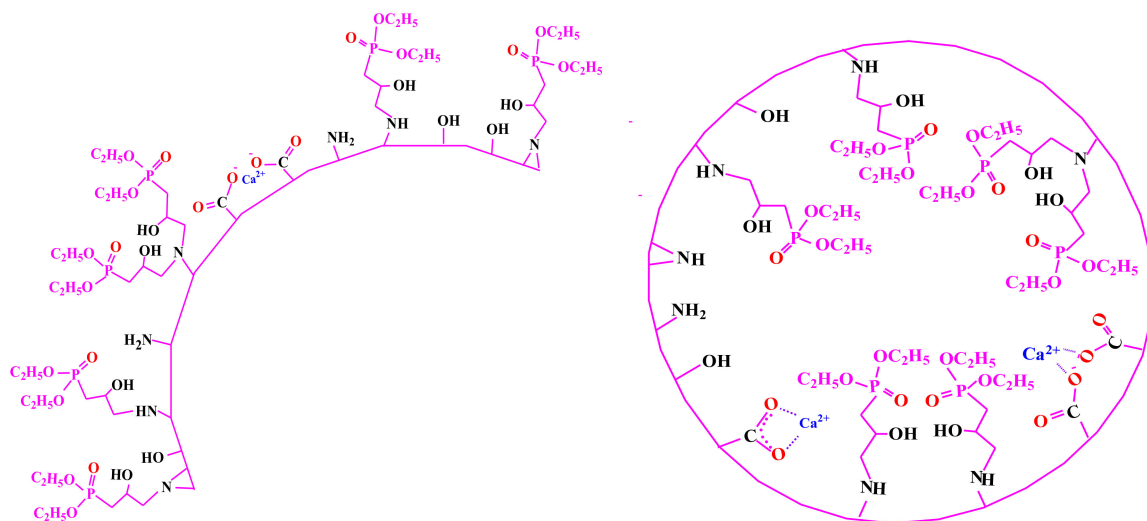
2.2.2. Synthesis of Activated APEI Beads (Methylene Chloride Grafted Spacer Arms)

Two grams of raw beads were immersed in 90 mL of ethanol:water (50:50; *v/v*) before adding 18 mL of epichlorohydrin drop-wise with gentle stirring, then the mixture was refluxed at 80 °C for 3 h. The reaction mixture was filtered off, stirred with ethanol for

24 h, then filtered again and dried in vacuum to give beads with active methylene chloride (spacer arm).

2.2.3. Phosphorylation of APEI Activated Beads (P2-APEI)

The produced active methylene chloride beads from the previous step were heated at 120–130 °C with 40 mL of triethyl phosphite for 24 h to produce phosphoryl group derivatives. The functionalized beads were filtered off and washed several times with ethanol and vacuum dried overnight. The size of the APEI beads was 2.8 ± 0.1 mm. Scheme 2 shows the functional groups present at the surface of the sorbent.



Scheme 2. Schematization of sorbent surface—functional groups.

2.3. Characterization of Materials

The morphology observation and the semi-quantitative surface analyses were obtained on a Phenom ProX scanning electron microscope (SEM, Thermo Fischer Scientific, Inc., Waltham, MA, USA) coupled with, energy dispersive X-ray analysis (EDX) facilities. The textural properties of the sorbents were qualified using the Barrett, Joyner and Halenda (BJH) method and a Micromeritics TrisStar II (Norcross, GA, USA). The pre-treatment of the samples consisted of their degassing at 100 °C for 12 h. A Netzsch STA 449 F3 Jupiter thermogravimeter was used for Thermal gravimetric analysis (TGA) analysis, with a temperature ramp of 10 °C/min (under oxygen or air atmosphere) (NETZSCH-Gerätebau GmbH, Selb, Germany). The elemental composition of the sorbents was obtained on a Vario EL cube element analyzer (Elementar Analysensysteme GmbH, Langenselbold, Germany). Fourier transform infrared spectra were collected on KBr discs by incorporation of dried ground samples with an IRTracer-100 (Shimadzu, Tokyo, Japan). X-ray photoelectron Spectroscopy (PS) spectra were acquired using an ESCALAB 250XI+ instrument (Thermo Fischer Scientific, Inc., Waltham, MA, USA). The pH-drift method was used to approach the pH_{PZC} of the materials [47]. A series of flasks containing 100 mg of material and 50 mL of 0.1 M NaCl solutions with an initial pH (pH_0) varying between 1 and 11 were stirred for 48 h. The equilibrium pH (pH_{eq}) was measured using a Mettler Toledo pH-meter (Mettler, Columbus, OH, USA). The pH_{PZC} was deduced from the titration curve considering pH_{PZC} as the pH verifying $\text{pH}_{\text{eq}} = \text{pH}_0$.

2.4. Sorption Tests

Sorption tests were performed with the batch method. A fixed amount of sorbent (m, g) was mixed with a fixed volume (V, L) of solution at a specific concentration (C_0 , mmol L^{-1}) and pH (variable for pH study, or optimized pH value, see below). The agitation was maintained at 170 rpm while the standard room temperature was $T: 21 \pm 1$ °C

(using a reciprocal shaker, Eyela NTS-4000C, Rikakikai Co. Ltd., Bunkyo City, Tokyo, Japan). After equilibrium (or fixed sampling times), the sample was collected and filtered through a filter membrane before analyzing metal content (C_{eq} , mmol L^{-1}) by ICP-AES (inductively coupled plasma atomic emission spectrometer, ICPS-7510 Shimadzu, Tokyo, Japan). The sorption capacity (q_{eq} , mmol g^{-1}) was deduced from concentration variation by the mass balance equation $q_{eq} = (C_0 - C_{eq}) \times V/m$. Similar procedures were used for investigating the sorption of REEs from multi-metal solutions (equimolar concentration: 1 mmol L^{-1}).

The tests for metal desorption were also performed in a batch reactor. The samples of sorbents loaded with metal ions were collected from uptake kinetic experiments. The eluent was an acidic calcium chloride solution (i.e., $0.2 \text{ M HCl}/0.5 \text{ M CaCl}_2$). The sorbent dosage (SD, g L^{-1}) was set at 0.8 g L^{-1} . In the investigation of sorbent recycling, a rinse was systematically performed between each step. The comparison of the amounts of metal sorbed and released was used for calculating the sorption capacity and the desorption efficiency.

The precise experimental conditions are systematically reported in the caption of the figures (see below).

The uptake kinetics and sorption isotherms were fitted by conventional equations summarized in Table S1a (pseudo-first order rate equation, PFORE; pseudo-second order rate equation, PSORE; resistance to intraparticle diffusion, RIDE) and Table S1b (Langmuir, Freundlich, and Sips equations) (see Supplementary Materials). The quality of curve fitting was evaluated using the determination coefficient (i.e., R^2) and the Akaike information criterion (AIC) [48].

2.5. Treatment of Ore Residues

The solid waste that was tested for the application of P2-APEI was collected from the tailing ponds of the Abu Thora mining site (Southwestern Sinai, Egypt). The local ores were initially subjected to acid leaching; these are mainly constituted of gibbsite-bearing shales. The residue collected on-site was exploited by pug leaching for extracting supplementary valuable metals. The curing temperature was set to $120 \text{ }^\circ\text{C}$.

The ore and waste residue were first digested using different acids (hydrofluoric, hydrochloric, and nitric acids). The leaching residue was removed by filtration, while the filtrate was adjusted to a final volume of 100 mL in a volumetric flask. The characterization of the leachate followed different methods. Aluminum, Ca, Fe, and Mg were analyzed by atomic absorption spectrometry (Unicam AAS-969 Vitech International BV, Geleen, The Netherlands); carbonate and phosphate analysis were processed by the Shapiro method [49]. Silica content was obtained by the molybdenum blue method and total REE concentration was evaluated by the Arsenazo III method (using Shimadzu UV-160 spectrophotometer, Shimadzu, Kyoto, Japan) [50]. Uranium was quantified by oxidimetric titration against ammonium metavanadate [51].

The complexity of the leachate and the presence of high concentrations of iron and aluminum required a pre-treatment of the solutions at pH 4 and 5 successively using 3 M NaOH solutions.

The sorption test was performed in batch with a sorbent dosage of 1 g L^{-1} and a contact time of 2 h . The pre-treated leachates were adjusted at different pH values to evaluate the optimum pH for the separation of REEs from base metals (i.e., pH: 1.38–3.91). After sorption, the sorbent was rinsed and dispersed in the eluent (i.e., $0.2 \text{ M HCl}/0.5 \text{ M CaCl}_2$); the sorbent dosage was set to 5 g L^{-1} .

The eluates were collected and REEs were precipitated at pH 1 using an oxalic acid solution (15% , w/w). The concentrations of metals in both the oxalate precipitate and the sorbent (cross-section) at the end of the process were semi-quantitatively determined using EDX facilities.

3. Results and Discussion

3.1. Characterization of Materials

3.1.1. Scanning Electron Microscopy (SEM) and SEM-EDX Characterizations

Table S2 shows the SEM pictures of the surface and cross-section for APEI, activated APEI (with epichlorohydrin, APEI-Cl), and P2-APEI. The surface was very dense for APEI and tended to be progressively more porous with the successive chemical modifications. On the other hand, The cross-sections were much more porous than the surfaces (especially for APEI and APEI-Cl); interconnected scaffolds can anticipate good mass transfer properties (after passing through the external “skin”). The chemical modifications contributed to altering the surface of the beads that became more porous at the level of the external layers. The heterogeneities between the surface and the internal porous network were confirmed by the differences in the semi-empirical analyses for the three materials. For APEI, the nitrogen and chlorine contents were higher in the cross-section than at the surface of the bead. In the case of APEI-Cl, in contrast, the nitrogen and chloride contents were higher at the surface of the sorbent, while the Ca content increased in the inner compartment of the bead. The immobilization of the phosphorous reactive groups was confirmed by the appearance of the P signal (with an atomic concentration in the range of 5–6% for both surface and cross-section). The percentages of N and Cl in P2-APEI decreased compared with the values reached with APEI and APEI-Cl. The concentration of O decreased between the surface and the inner compartment by around 6% for APEI and P2-APEI; this difference was less marked for APEI-Cl. These results show that the APEI sorbent is heterogeneous and that the functionalization of the support does not significantly change this trend.

3.1.2. Textural Properties

Figure S1 (see Supplementary Materials) compares the S_{BET} surfaces of APEI and P2-APEI: the functionalization of the beads led to a ~10% decrease in the specific surface area and the reduction in the porous volume (by 10–12%) while the pore size slightly increased (by 5–12%). This is consistent with the SEM observations: the larger pores of P2-APEI contribute to explaining the lower specific surface area.

3.1.3. Thermogravimetric Analysis

Figure S2 summarizes the weight losses of the two sorbents submitted to increasing temperatures (TGA analysis under O_2 atmosphere). APEI and P2-APEI showed very similar TGA profiles. It is noteworthy that the water content was higher in APEI than in P2-APEI: the weight loss in the first segment (below 173 or 148 °C), which represents water release, was more intense for APEI, about 11% vs. ~4% for P2-APEI. The highest weight losses were observed at 305 °C and 550 °C (identified on DrTG curves) for APEI. In the case of P2-APEI, the weight loss profiles were more smoothed and more steps could be detected: the DrTG profile identified four successive maxima at 303, 475, 630, and 724 °C. The functionalization of the support increased its stability. For APEI, weight loss above 600 °C was negligible, the thermal degradation was only stabilized at 750 °C for P2-APEI. The positive effect of the incorporation of phosphorous compounds in materials on their thermal stability has frequently been reported [52]. The two new peaks in the DrTG curve may be assigned to the presence of the spacer-arm and activated agent (the first step in the functionalization of APEI), and phosphorus-based compounds, respectively. The final residue (above 800 °C) represented about 9.7% for APEI and 11.6% for P2-APEI.

3.1.4. FTIR Analysis

Figure 1 reports the FTIR spectra of raw APEI beads, activated APEI beads, and phosphorylated beads. The main typical reactive groups were identified with their respective fingerprints. Table S3 reports the corresponding wavenumbers and the assignments of their respective vibrations while Figure S3 shows a focus of these spectra on specific wavenumber ranges. Briefly, the broad and poorly resolved band in the range 3700–3100 cm^{-1} represents the contributions of stretching vibrations for –OH, –NH, and –NH₂ bonds.

The three spectra were roughly the same: APEI-Cl showed a broader spectrum with an increased contribution at around 3250 cm^{-1} . The activation of APEI beads with epichlorohydrin grafting was confirmed by the strong peak at 788 cm^{-1} and the shift in the C–C and C–O–C, or C–O stretching vibrations from 1095 cm^{-1} to 1089 cm^{-1} . After functionalization, this peak disappeared: the phosphorylation was highly efficient and quantitative. Obviously, the phosphorylation was accompanied by the appearance of a series of peaks corresponding to P=O (asymmetric stretching at 1251 cm^{-1}), P(O) stretching (phosphate, at 1033 cm^{-1}), and P–O–C stretching (at 611 cm^{-1} and 746 cm^{-1}). In addition, a new peak appeared at 1741 cm^{-1} (assigned to C(=O)O ester stretching in alginate). In the original material and activated APEI-Cl, this peak was overlapped with C=N (GA interaction with amine groups PEI). After deconvolution, apparently, the peak split into two components corresponding to C=N and C=O from carboxylate because of the reduced contribution of specific N–H groups (in the overlapping).

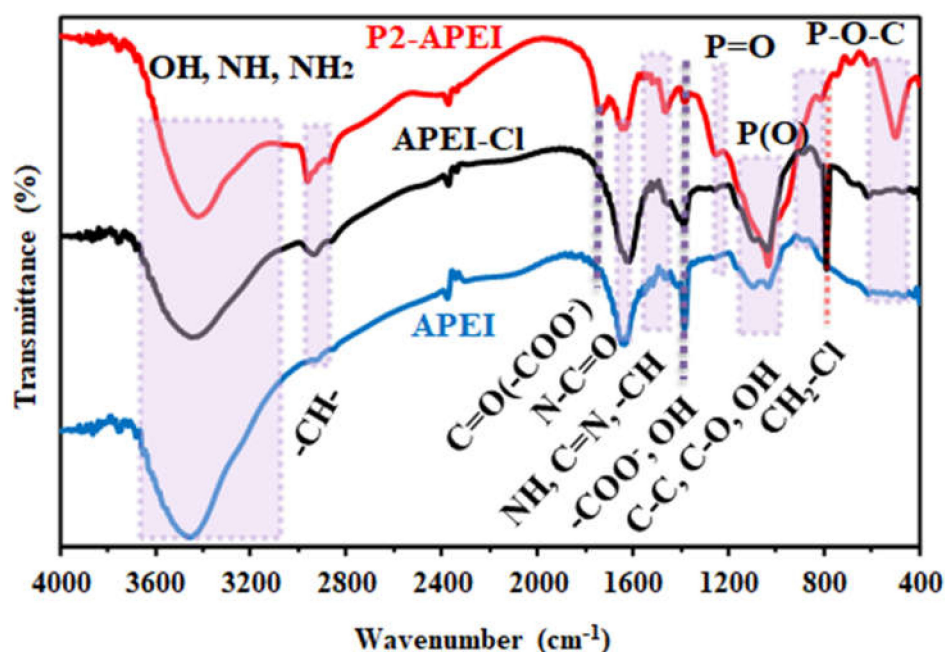


Figure 1. Fourier transform infrared (FTIR) spectra of APEI, APEI-Cl, and P2-APEI materials.

After metal sorption, the FTIR spectra were changed (Figure 2, Figure S4, and Table S4). The relative intensity of the band at 1741 cm^{-1} was reduced. The peak at 1384 cm^{-1} was completed by a shoulder at $1408\text{--}1404\text{ cm}^{-1}$, which can be assigned to carboxylate salt. This is confirmation that metal ions, at least partially, interact with carboxylate by ion-exchange with Ca(II). A new band appeared at 617 cm^{-1} , which can be attributed to the sulfate anion. This means that the sorption of REEs involves the binding of a metal sulfate complex. The new peak at $1103\text{--}1111\text{ cm}^{-1}$ may be associated with the interaction of metal ions with P(O) (stretching vibration of phosphate) and/or the stretching of C–N. These results confirm that phosphate and amine groups contribute to metal binding. The contribution of amine is also correlated to the widening of the band at $3700\text{--}3100\text{ cm}^{-1}$.

It is noteworthy that the desorption of the metals (considered in relevant figures after five cycles of re-use) allowed for reversing the appearance of these new peaks. The desorption roughly restored the FTIR spectra of metal-loaded P2-APEI to the original spectrum of the sorbent, with the remarkable exception of the peak at 498 cm^{-1} , assigned to polysulfide (S–S stretching band attributed to fucoidan, overlapped with P–O–C band) that disappeared after sorption and desorption. The relative intensity of some peaks was not completely recovered; for example, the peak at 1741 cm^{-1} . The peak at $1103\text{--}1011\text{ cm}^{-1}$ also remained partially after metal desorption. The procedure of sorption/desorption

appears to be efficient for restoring the material, although some chemical modifications cannot be neglected based on the changes in the FTIR spectra.

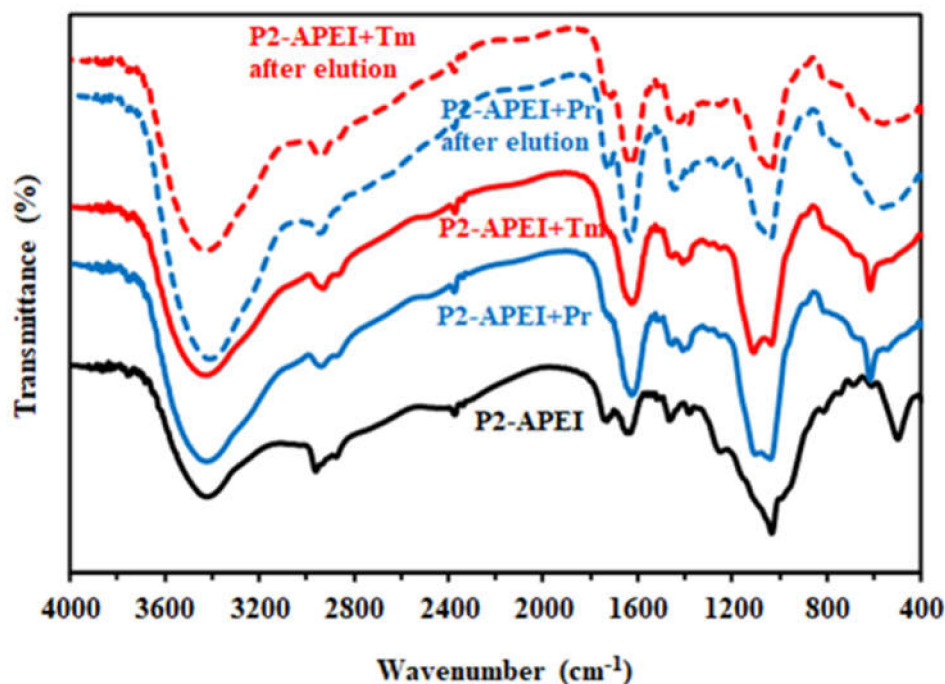


Figure 2. FTIR spectra of P2-APEI, P2-APEI sorbent loaded with Pr(III) and Tm(III), and after metal desorption.

3.1.5. XPS Analysis

The XPS survey scan (Figure 3) brings new evidence for the successful functionalization of APEI. The typical P 2p and P 2s signals appeared at binding energies (BEs) 133 and 190 eV, respectively. The weak signal at 348 eV, which is assigned to Ca 2p, almost disappeared after phosphorylation as well as S 2p and S 2s signals at 167 and 228 eV, respectively.

The sorption of REEs is identified by the appearance of their typical signals. The most significant for Pr(III) appeared around 118 eV (Pr 4d), 221, and 234 eV (Pr 4p_{3/2} and Pr 2p_{1/2}), 308 eV (Pr 4s), 934, and 955 eV (Pr 3d_{5/2} and Pr 3d_{3/2}), and 1245/1340 eV (Pr 3p_{3/2} and Pr 3p_{1/2}). In the case of Tm-loaded sorbent, the typical signals were identified at 32 eV (Tm 5p_{1/2}), 178 eV (Tm 4d), 335 eV (Tm 4p_{3/2}), and 473 eV (Tm 4s).

High-resolution XPS spectra are summarized in Table S5. Table S5b–d compare the respective spectra for APEI and P2-APEI as well as the spectra for the functionalized sorbent after Pr(III) and Tm(III) sorption. Table S5a shows that the profiles of the C 1s signal was significantly affected by the functionalization of the raw material and even more by the binding of Pr(III) and Tm(III): more specifically, the contribution of C–C signal is reinforced. Table S5b shows that the sorption of REEs was followed by the reinforcement of the contribution of the signal at ~530 eV (assigned to P=O) after metal binding, while the C=O signal was reduced; the contribution of carboxylate groups to metal uptake cannot be neglected. In the case of N 1s (Table S5c), the peak at BE ~399.4 eV (associated with N–C=O, N–H, N–C) apparently disappeared, while the R=N–R band was increased (the intensity of the other band at ~400.5 eV decreases). The N-based functional groups are involved in metal binding. Table S5d confirms the changes in the environment of P-bearing groups after the sorption of REEs. Table S5e summarizes the assignments and BEs of C 1s, O 1s, N 1s, and P 2p signals (representative of the most relevant functional groups identified on the two sorbents) as well as their atomic fractions. One of the first pieces of information derived from this table is the relative stability of the BEs: the Δ BEs did not exceed 0.3 eV in most cases. The most significant differences are reported in terms of atomic fractions and

the appearance/disappearance of deconvoluted peaks. The atomic fractions confirm the conclusions raised while observing the changes in HRES XPS spectra.

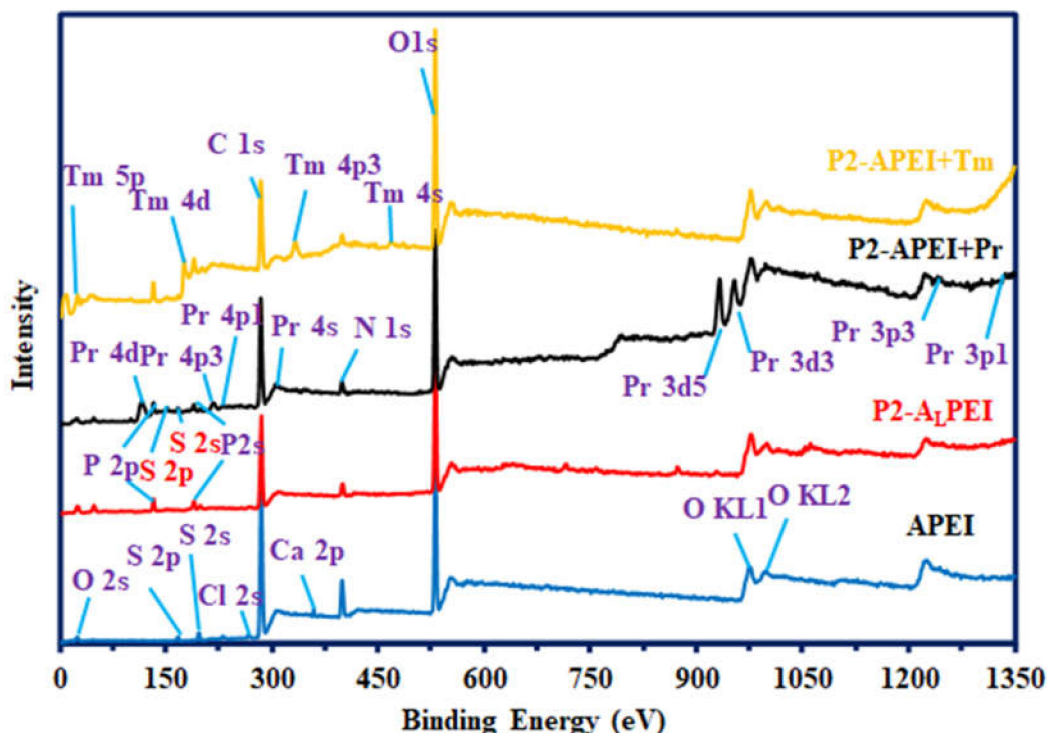


Figure 3. XPS survey scans of APEI and P2-APEI beads (including after Pr(III) and Tm(III) sorption).

3.1.6. Elemental Analysis and pH_{PZC}

Table S6 shows the elemental analysis of APEI before and after functionalization. The chemical modification (epichlorohydrin activation and grafting of triethyl phosphite) led to a decrease in the relative fraction of nitrogen in the sorbent: from $4.18 \text{ mmol N g}^{-1}$ to $2.76 \text{ mmol N g}^{-1}$. The phosphorylation allowed a phosphorus content close to 2.58 mmol g^{-1} to be reached. This means that about 93.5% of N-based groups were grafted with triethyl phosphite: the functionalization procedure was highly efficient.

The pH_{PZC} , approached by the pH-drift method, was strongly reduced by the chemical modification from 6.6 for APEI to 2.4 for P2-APEI (Figure S5). These values can be explained by the reactive groups present at the surface of the sorbent: APEI bears primary, secondary, and tertiary amine groups from PEI (pK_a : 4.5, 6.7, and 11.6, respectively [53]) and carboxylic groups (mannuronic and guluronic groups from alginate with pK_a : 3.38 and 3.65, respectively [54]). Additionally, P2-APEI holds phosphonate moieties with pK_a values supposed to be much higher [55], depending on the substituting groups on the phosphonate entity. The order of magnitude of the pH_{PZC} is consistent with the value reported for polyaminophosphonic acid-functionalized poly(glycidyl methacrylate) (i.e., 2.69) [28] and a composite obtained by high-energy ball milling of magnetite with aminophosphonic derivative of PGMA (i.e., 2.83) [56]. The functionalized sorbent will be deprotonated on a wider pH range than the raw material: the repulsion of metal cations is expected to be decreased for P2-APEI in weakly acidic solutions.

3.2. Sorption Studies on Synthetic Solutions

3.2.1. pH Effect

Figure 4 compares the effect of equilibrium pH on the sorption properties of APEI and P2-APEI (initial pH varies between 1 and 5) for both Pr(III) and Tm(III). The duplication of experiments shows the good reproducibility of sorption performance. In the case of APEI,

the sorption capacity linearly increased with the pH; however, under selected experimental conditions, the improvement in sorption performance remained limited: from 0.025 to 0.082 mmol Pr g⁻¹ and from 0.013 to 0.051 mmol Tm g⁻¹. The effect of pH on the sorption of REEs was more marked in the case of P2-APEI. While the sorption capacities were of the same order of magnitude as APEI at pH close to 1 (i.e., 0.053 mmol Pr g⁻¹ and 0.03 mmol Tm g⁻¹), the binding strongly increased with the pH: up to 0.36 mmol Pr g⁻¹ and 0.27 mmol Tm g⁻¹ (i.e., seven and nine times the reference values for APEI).

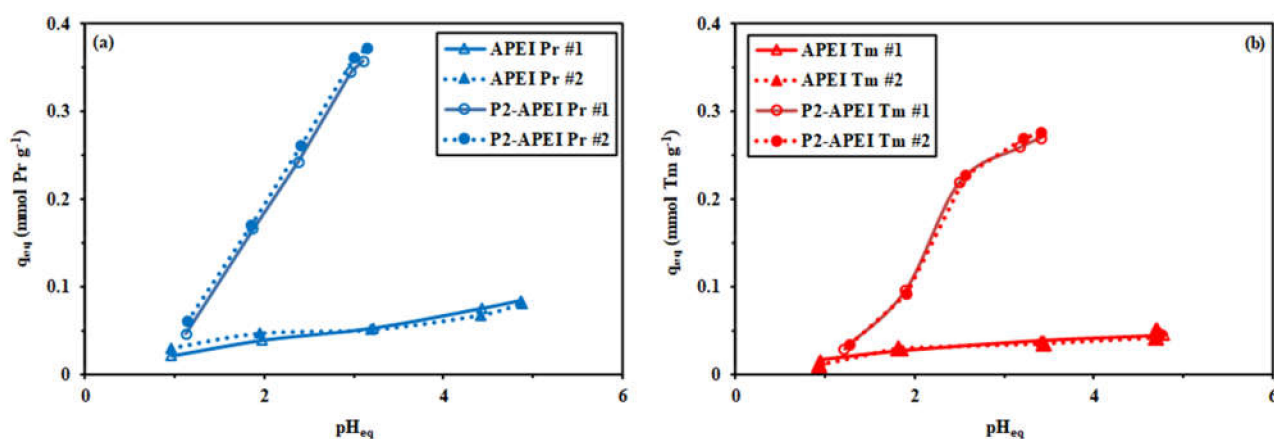


Figure 4. Effect of equilibrium pH on the sorption of Pr(III) (a) and Tm(III) (b) using APEI and P2-APEI sorbents (C_0 : 50 mg L⁻¹; Sorbent dosage, SD: 1 g L⁻¹; Contact time: 48 h; T: 22 ± 1 °C; duplicate experiments).

The progressive deprotonation of the sorbents increases their sorption efficiency; this is especially significant in the case of P2-APEI because of the differences in pH_{PZC} values and the presence of phosphonate groups. In acidic pH solutions, alginate carboxyl groups are under their acidic form, while all amine groups are also protonated: cations are repulsed. On the other hand, for P2-APEI, the positive charge at the surface of the sorbent tends to decrease, favoring metal binding; above pH 2.4, the surface of the sorbent becomes progressively negative. Precisely, the sorption of Tm(III) drastically increases above pH 2.5.

The speciation diagrams for Pr(III) and Tm(III) are reported in Figure S6. At pH below 3, the predominant species were the sulfate complexes (REE(SO₄)⁺ and REE(SO₄)₂⁻): the contribution of the anionic species decreased with increasing the pH. The protonated species (free REE³⁺ and REE(SO₄)⁺) also predominated over the whole pH range. Anionic species at pH 1 can be bound onto protonated amine groups by electrostatic attraction. The increase in S content on the sorbent after pH sorption means that REE sulfate species are involved in metal binding. Between pH 2 and pH 4, the fraction of free REE(III) progressively increased and predominated over pH 3.8. This may be correlated to the strong enhancement in sorption property at pH above 2, especially for P2-APEI.

Figure S6 follows the pH variation during metal sorption for APEI and P2-APEI sorbents. The differences in acid–base properties of the sorbents were consistent with those variations: APEI tended to slightly increase the pH of the solution in the range pH_0 2–4 (maximum variation: +0.7 pH unit) while P2-APEI progressively decreased the pH of the solution (by up to −1.6/−1.85). This is another illustration of the difference in the sorption mechanisms for the two sorbents.

3.2.2. Uptake Kinetics

The uptake kinetics are represented in Figures 5 and 6. Under selected experimental conditions (C_0 : 50 mg L⁻¹ and SD: 0.25 g L⁻¹), the sorption process was fast enough to reach equilibrium within 30 min of contact (Figure 5) in mono-component solutions for both APEI and P2-APEI sorbents. Similar trends were observed for Pr(III) and Tm(III) uptake from binary solutions. As expected, the enhanced affinity of P2-APEI for REEs

allowed for a substantial increase in the sorption capacity and efficiency (illustrated by lower residual concentrations).

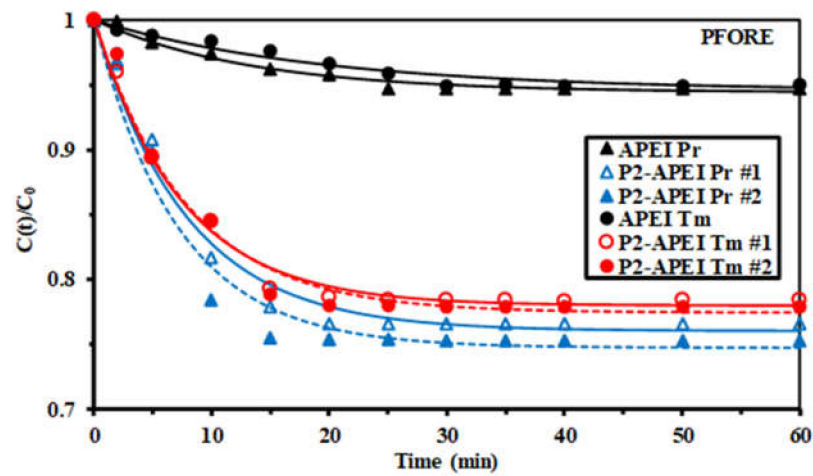


Figure 5. Pr(III) and Tm(III) uptake kinetics using APEI and P2-APEI sorbents (duplicate experiments) (C_0 : 50 mg L^{-1} ; Sorbent dosage, SD: 0.25 g L^{-1} ; pH_0 : 5; pH_{eq} : 4.87 and 4.62 for APEI for Pr(III) and Tm(III), respectively; 3.24–3.12 for Pr(III) and 3.44–3.47 for Tm(III) with P2-APEI; T: $22 \pm 1 \text{ }^\circ\text{C}$; solid lines: modeling with PFORE).

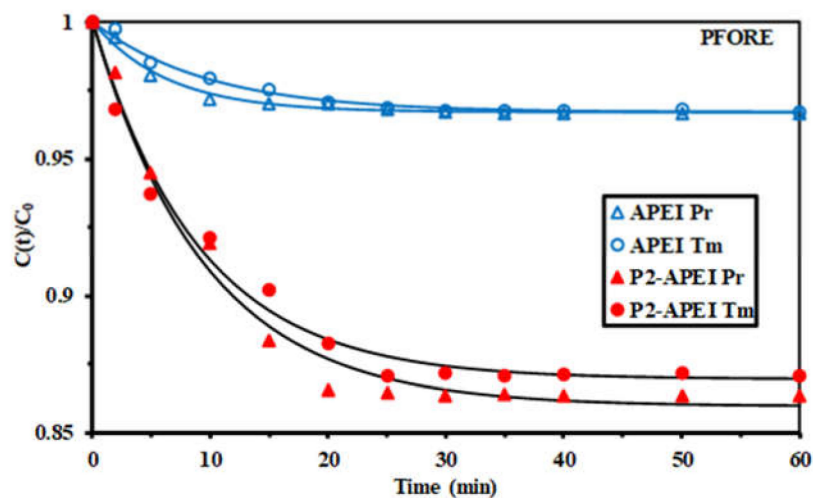


Figure 6. Pr(III) and Tm(III) uptake kinetics using APEI and P2-APEI sorbents from binary solutions (C_0 : 50 mg L^{-1} ; Sorbent dosage, SD: 0.25 g L^{-1} ; pH_0 : 5; pH_{eq} : 4.87 and 4.62 for APEI for Pr(III) and Tm(III), respectively; 3.24–3.12 for Pr(III) and 3.44–3.47 for Tm(III) with P2-APEI; T: $22 \pm 1 \text{ }^\circ\text{C}$; solid lines: modeling with PFORE).

Sorption capacity for P2-APEI was over four times the value reached for APEI. The kinetic profiles were fitted with selected models (reported in Table S1) [57,58]. The comparison of determination coefficients and Akaike information criterion (AIC, Table S1b) for the different equations showed that the best fits were obtained with the pseudo-first order rate equation (Tables 1 and 2).

Table 1. Pr(III) uptake kinetics using APEI and P2-APEI sorbents—fitting parameters for the PFORE, PSORE, and RIDE models.

Model	Parameter	Sorbent		
		APEI	P2-APEI	
			1st Run	2nd Run
Exp. PFORE	$q_{eq,exp}$ (mmol g ⁻¹)	0.0795	0.357	0.348
	$q_{1,calc}$ (mmol g ⁻¹)	0.0828	0.365	0.356
	$k_1 \times 10^2$ (min ⁻¹)	7.45	12.8	14.0
	R ²	0.980	0.985	0.973
	AIC	-133	-102	-94
PSORE	$q_{2,calc}$ (mmol g ⁻¹)	0.101	0.418	0.405
	$k_2 \times 10$ (L mmol ⁻¹ min ⁻¹)	7.95	3.81	4.35
	R ²	0.965	0.956	0.938
	AIC	-126	-90	-85
	RIDE	$D_e \times 10^8$ (m ² min ⁻¹)	3.66	4.91
	R ²	0.960	0.960	0.945
	AIC	-124	-92	-87

Table 2. Tm(III) uptake kinetics using APEI and P2-APEI sorbents—fitting parameters for the PFORE, PSORE, and RIDE models.

Model	Parameter	Sorbent		
		APEI	P2-APEI	
			1st Run	2nd Run
Exp. PFORE	$q_{eq,exp}$ (mmol g ⁻¹)	0.0608	0.271	0.269
	$q_{1,calc}$ (mmol g ⁻¹)	0.0666	0.276	0.275
	$k_1 \times 10^2$ (min ⁻¹)	5.09	13.5	12.7
	R ²	0.964	0.992	0.985
	AIC	-130	-113	-104
PSORE	$q_{2,calc}$ (mmol g ⁻¹)	0.085	0.313	0.315
	$k_2 \times 10$ (L mmol ⁻¹ min ⁻¹)	5.67	5.64	5.06
	R ²	0.953	0.969	0.960
	AIC	-125	-98	-93
	RIDE	$D_e \times 10^8$ (m ² min ⁻¹)	2.74	5.16
	R ²	0.933	0.975	0.964
	AIC	-122	-101	-95

Figure S8 shows the modeling of kinetic profiles with alternative models (PSORE and RIDE). This was also confirmed by the close values for calculated equilibrium sorption capacities and experimental values: overestimation reached 2% for P2-APEI and 4% for APEI. The solid lines in Figure 5 represent the PFORE fitting applied to the experimental profiles as confirmation of the appropriateness of the model to describe the transfer of the REEs onto the sorbents. The PFORE is generally associated with a physical sorption mechanism. However, Hubbe et al. [59] pointed out the importance of selecting appropriate experimental conditions for justifying the relevant interpretations of mathematical fits. They also demonstrated that the fitting of kinetic profiles was frequently correlated to sorption processes controlled by resistance to intraparticle diffusion. The apparent rate coefficient (i.e., k_1) was more than doubled for P2-APEI compared with the reference value (i.e., APEI) for both Pr(III) and Tm(III). The faster kinetics of P2-APEI can be correlated to the more open surface structure observed in the SEM pictures (Table S2). Table S7 shows the surface and crosscut section SEM pictures (with their relevant semi-quantitative EDX analyses). Metal sorption slightly changes the surface of APEI beads with the formation of additional porosity; internal porosity was not affected. In the case of P2-APEI and the surface morphology was not significantly changed. The semi-quantitative analyses

confirmed the higher sorption of REEs in P2-APEI. It is noteworthy that the distribution of elements (REE, N) was more homogeneous between the surface and crosscut section for P2-APEI for Tm(III) than for Pr(III). It is noteworthy that in this case, the Pr(III) content was remarkably lower in the crosscut section for P2-APEI.

Although the RIDE (resistance to intraparticle diffusion, the so-called Crank equation [57]) model, does not fit experimental profiles as well as the PFORE model, the equation allows an approximate value of the effective diffusivity (i.e., D_e) to be calculated. As expected, the diffusivity slightly increased with the functionalization of the sorbent from 3.7×10^{-8} to $5.1 \times 10^{-8} \text{ m}^2 \text{ min}^{-1}$ for Pr(III), and from 2.7×10^{-8} to $5.0 \times 10^{-8} \text{ m}^2 \text{ min}^{-1}$ for Tm(III). Praseodymium was characterized by a larger size of hydrated ion (i.e., $r_h = 1.179 \text{ \AA}$) compared with Tm(III) (i.e., $r_h = 0.994 \text{ \AA}$) [60]. This is not enough to affect the mass transfer properties in the sorbents. These values of D_e were of the same order of magnitude as the self-diffusion of Pr(III) and Tm(III) in water (i.e., 3.7×10^{-8} and $3.5 \times 10^{-8} \text{ m}^2 \text{ min}^{-1}$, respectively [61]). This means that the resistance to intraparticle diffusion does not play a critical role in the control of uptake kinetics. This is consistent with the fast sorption (equilibrium reached within 30 min), despite the relatively large size of the beads (i.e., 2.8–2.9 mm).

Similar trends were observed for uptake kinetics in binary solutions (Figure 6 and Table 3). The effective diffusivities were of the same order of magnitude than for mono-component solutions (ranging between 4.4×10^{-8} and $6.7 \times 10^{-8} \text{ m}^2 \text{ min}^{-1}$). It is noteworthy that the sorption capacities at equilibrium in binary solutions were lower than the values reported (for the same initial metal concentration) in the case of mono-component solutions. The cumulative sorption capacity was close to $0.38 \text{ mmol REE g}^{-1}$ ($0.196 \text{ mmol Pr g}^{-1} + 0.186 \text{ mmol Tm g}^{-1}$) while for individual metal solutions, the sorption capacities were $0.36 \text{ mmol Pr g}^{-1}$ and $0.275 \text{ mmol Tm g}^{-1}$ for PFORE modeling of REE sorption using P2-APEI. The competition effect decreased the global sorption performance. This was also shown by the decrease in the apparent rate coefficient by one order of magnitude. The two metals were supposed to be bound on the same reactive groups. The cumulative sorption capacity was far below the maximum sorption capacities (see below); this means that the sorbent was not saturated. Both the global sorption capacity and the kinetic rates were depreciated by the competitor effect.

Table 3. Pr(III) and Tm(III) uptake kinetics using APEI and P2-APEI sorbents from binary solutions—fitting parameters for the PFORE, PSORE, and RIDE models.

Model	Parameter	Sorbent			
		APEI		P2-APEI	
		Pr(III)	Tm(III)	Pr(III)	Tm(III)
Exp. PFORE	$q_{eq,exp}$ (mmol g^{-1})	0.047	0.046	0.190	0.184
	$q_{1,calc}$ (mmol g^{-1})	0.047	0.047	0.196	0.186
	$k_1 \times 10^2$ (min^{-1})	1.59	1.02	1.05	1.10
	R^2	0.987	0.988	0.988	0.988
	AIC	−154	−154	−119	−123
PSORE	$q_{2,calc}$ (mmol g^{-1})	0.053	0.055	0.228	0.212
	$k_2 \times 10$ (L mmol^{-1} min^{-1})	39.7	22.5	5.62	6.91
	R^2	0.974	0.978	0.968	0.982
	AIC	−145	−145	−107	−118
	RIDE	$D_e \times 10^8$ ($\text{m}^2 \text{ min}^{-1}$)	6.72	4.55	4.43
R^2		0.976	0.978	0.970	0.985
AIC		−149	−147	−108	−122

The sorption of Pr(III) and Tm(III) controlled for both APEI and P2-APEI is not controlled by the resistance to intraparticle diffusion. The kinetic profiles can be described by the PFORE. This result was consistent with the conclusions raised for other deriva-

tives of APEI (quaternized, sulfonated, amidoximated) in the sorption of different metal ions [44–46,62,63].

3.2.3. Sorption Isotherms

Figure 7 shows the sorption isotherms for Pr(III) and Tm(III) using APEI and P2-APEI sorbents at pH_0 5. The duplication of the sorption isotherm for P2-APEI confirmed the good reproducibility of sorption performance. Equilibrium pH value varied between 4.7 and 4.8 for APEI but decreased to 3.1–3.5 for P2-APEI, consistently with the results reported for the study of the pH effect.

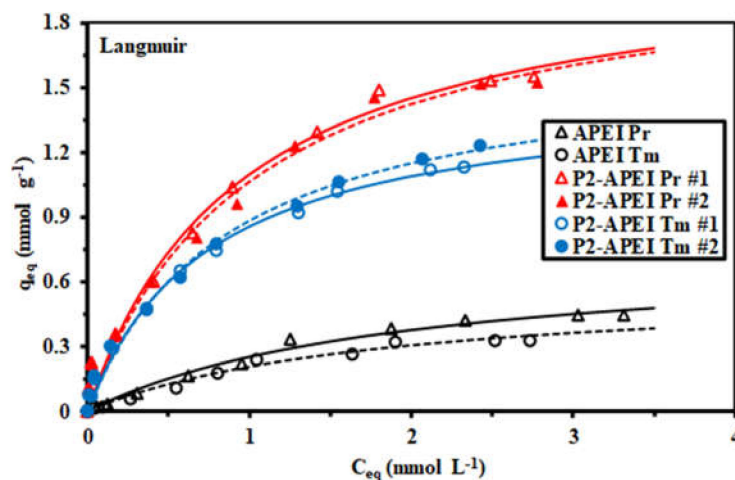


Figure 7. Pr(III) and Tm(III) sorption isotherms using APEI and P2-APEI (duplicate experiments) (C_0 : 10–500 mg L^{−1}; Sorbent dosage, SD: 0.5 g L^{−1}; pH_0 : 5; pH_{eq} : 4.81–4.7 and 4.79–4.72 for APEI for Pr(III) and Tm(III), respectively; 3.27–3.08 for Pr(III) and 3.54–3.39 for Tm(III) with P2-APEI; time: 48 h; T: 22 ± 1 °C; solid lines: modeling with the Langmuir equation).

The maximum sorption capacities reached 0.45 mmol Pr g^{−1} and 0.33 mmol Tm g^{−1} for APEI. The functionalization strongly increased the sorption capacities up to 1.54 mmol Pr g^{−1} and 1.19 mmol Tm g^{−1} (i.e., about three times). The highest sorption capacities for Pr(III) compared with Tm(III) showed the preference of the sorbent for light vs. heavy REE. The solution electronegativity of REEs can be ranked according to Pr(III) (3.037) < Tm(III) (3.503). Marcus [61] summarized the polarizability of elements using different sources that systematically report higher polarizability for Pr(III) than for Tm(III), combined with the lowest hydrated radius of Tm(III) (0.994 Å) than that of Pr(III) (1.179 Å), thulium may be considered a stronger acid than praseodymium, according to Pearson’s rules (hard and soft acid-base theory, (HSAB) [64]). Iftexhar et al. [65] compared the sorption of a series of REEs on biopolymer-layered double hydroxides LDH hybrid nanocomposites and they concluded that small ionic radii enhanced the sorption; this is contradictory to the trend found with P2-APEI (ionic radii: 1.179 Å for Pr(III) and 1.052 Å for Tm(III)). Phosphonate and amine groups are both considered hard bases [66,67], which are supposed to be more reactive with hard acids. In the case of strong cation exchange resin Dowex 50, Surls and Choppin [68] obtained a linear correlation between the ion-exchange sorbability (the energy of formation of the complex) and the ionic conductance of the REEs (and Am + Cu). Marcus [61] reported the conductivity of Pr(III) and Tm(III) to be 208.8 and 196.2 cm² Ω^{−1} mol^{−1}, respectively (reciprocal trend than the hydrated radius).

The shape of the curves was characterized by a steep initial increase in the sorption capacities followed by a saturation plateau. This shape is consistent with the asymptotic trend of the Langmuir equation compared with the Freundlich equation, which is assimilated to a power-type function. These conventional models (described in Table S1b) are commonly used for describing sorption isotherm profiles. The Langmuir equation supposes that the sorption occurs as a monolayer at the surface of the sorbent with no interactions between

the sorbed molecules. Furthermore, the energies involved in the sorption are considered homogeneous. The co-existence of different reactive groups (i.e., amine, carboxylate, and phosphonate) does not appear to create heterogeneities in terms of interaction with REEs. The Sips equation is a combination of the Langmuir and the Freundlich equation, which includes a third-adjustable parameter that is supposed to improve mathematical fitting (Figure S9).

Actually, Table 4 shows that there is no clear evidence for better fitting experimental profiles with the Sips equation (this depends on the couple metal/sorbent). The Langmuir equation, which is more mechanistic than the mathematical Sips function, was preferred for simulating isotherms in Figure 7. It is noteworthy that the models well fit the isotherm profile for residual concentrations higher than 0.2 mmol L⁻¹, but tended to underestimate the sorption capacities for the concentrations below 0.0 mmol L⁻¹. The comparison of $q_{m,L}$ and $q_{m,exp}$ showed that the model overestimated the experimental value of the sorption capacity at saturation by 68–76% for APEI, ~40%, and ~33% for P2-APEI and Pr(III)/Tm(III), respectively. The affinity coefficient (i.e., b_L) was slightly higher for P2-APEI (i.e., 0.98 to 1.33 L mmol⁻¹) than for APEI (i.e., 0.50–0.54 L mmol⁻¹). The affinity coefficients of the sorbents for Tm(III) were systematically a little better for Tm(III) than for Pr(III). The initial slope of the curve is described by the term $q_{m,L} \times b_L$ (L g⁻¹): 0.38 and 0.26 L g⁻¹ for Pr(III) and Tm(III) in the case of APEI, and 2.18 and 1.95 L g⁻¹ for P2-APEI.

Table 4. Pr(III) and Tm(III) sorption isotherms using APEI and P2-APEI sorbents—fitting parameters for the Langmuir, Freundlich, and Sips equations.

Model	Parameter	Sorbent						
		APEI		P2-APEI				
		Pr(III)	Tm(III)	Pr(III) #1	Pr(III) #2	Tm(III) #1	Tm(III) #2	
Exp.	$q_{m,exp}$	0.448	0.331	1.554	1.525	1.135	1.230	
	Langmuir	$q_{m,L}$	0.752	0.584	2.14	2.151	1.494	1.645
		b_L	0.502	0.539	1.05	0.980	1.334	1.153
		R^2	0.988	0.983	0.990	0.989	0.996	0.994
Freundlich	AIC	−81	−84	−55	−54	−70	−67	
	k_F	0.235	0.191	1.02	0.998	0.794	0.820	
	n_F	1.635	1.580	2.105	2.060	2.104	1.992	
	R^2	0.968	0.966	0.984	0.985	0.994	0.995	
Sips	AIC	−71	−76	−52	−53	−70	−71	
	$q_{m,S}$	0.540	0.392	2.867	3.161	2.269	2.749	
	b_S	0.922	1.21	0.597	0.488	0.572	0.447	
	n_S	0.666	0.621	1.319	1.380	1.422	1.441	
	R^2	0.994	0.991	0.990	0.989	0.998	0.998	
	AIC	−84	−83	−53	−53	−80	−80	

Table 5 reports the Pr(III) and Tm(III) sorption characteristics for a series of alternative sorbents. Most of the studies investigated the sorption of REEs in the pH range of 3–5. Taking into account both the kinetic criterion (i.e., equilibrium time) and the maximum sorption capacity (i.e., $q_{m,L}$), P2-APEI appeared to be one of the most efficient sorbent. The functionalized sorbent showed remarkably fast kinetics (20–30 min for reaching equilibrium) and outstanding sorption capacities (1.57 mmol Tm g⁻¹ and 2.14 Pr g⁻¹). The most efficient sorbents showed comparable sorption capacity; for example, 2.08 mmol Pr g⁻¹ in the case of sulfonic resin D72, but at the expense of much slower kinetics (equilibrium 24 h) [10]. In the case of Tm(III), the most competitive sorbent was *Turbinaria conoides*, with a sorption capacity that did not exceed 1.19 mmol Tm g⁻¹ and a longer required contact time (more than 3 h for reaching equilibrium). Therefore, P2-APEI appears to be a good compromise between sorption capacity and kinetic criteria and a promising sorbent for LREEs and HREEs. The main weakness of this sorbent consists of the relatively weak

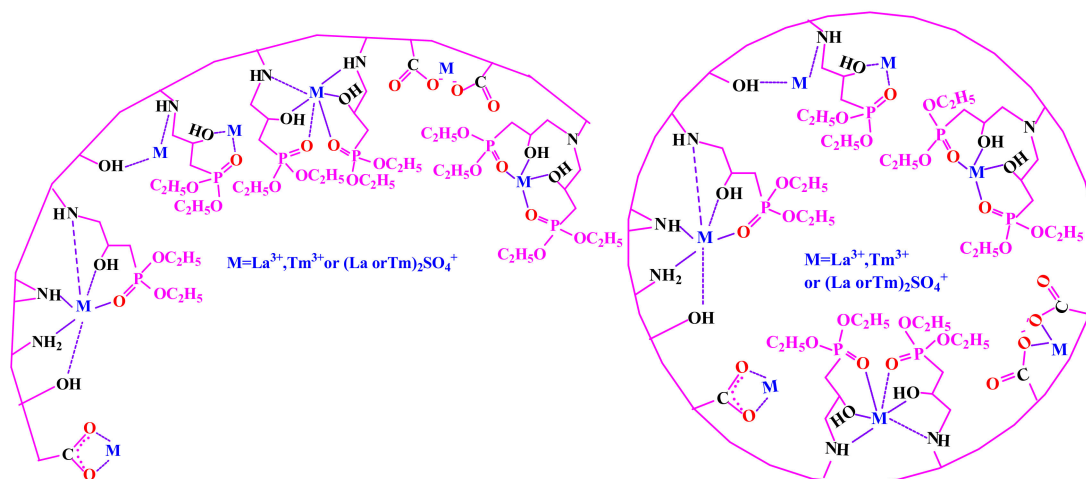
affinity coefficient (i.e., $b_L \sim 1\text{--}1.3 \text{ L mmol}^{-1}$), while the best other sorbents showed values close to 8.6 or 17.1 L mmol^{-1} .

Table 5. Comparison of the Pr(III) and Tm(III) sorption properties for alternative sorbents.

Metal	Sorbent	pH	t_{eq} (min)	$q_{m,L}$ (mmol g ⁻¹)	b_L (L mmol ⁻¹)	Ref.
Pr(III)	<i>Pseudomonas aeruginosa</i>	5	240	0.94	n.r.	[69]
	D72 resin (–SO ₃ H)	3	1440	2.08	8.60	[10]
	<i>Turbinaria conoides</i>	5	90	1.04	7.33	[70]
	<i>T. conoides</i> /polysulfone beads	5	240	0.85	2.40	[70]
	Crab shell	5	35	0.47	3.66	[71]
	Orange peel	5	50	0.42	2.25	[71]
	<i>Laminaria digitata</i> beads	4	180 (FD) 1440 (AD)	0.89	125.4	[72]
	<i>Laminaria digitata</i> foams	4	1440	0.79	111.3	[72]
	APEI	5	30	0.75	0.50	This work
	P2-APEI	5	20	2.14	1.02	This work
Tm(III)	PAN-polyurethane foam	7.5	40	0.0083	51.1	[73]
	<i>Turbinaria conoides</i>	5	200	1.19	17.1	[74]
	<i>T. conoides</i> /polysulfone beads	5	200	0.93	5.91	[74]
	Zr-ion imprinted xanthan gum-layered double hydroxide	4	80	0.19	255.1	[75]
	APEI	5	30	0.58	0.54	This work
	P2-APEI	5	20	1.57	1.24	This work

3.2.4. Sorption Mechanism

According to the data collected from pH_{pzc} (deprotonation of the sorbent), EDX analysis (the presence of metal and S elements), FTIR analysis (presence of sulfate group, shifts of specific groups after sorption), and speciation diagrams (free metal and metal complex species), it is probable that metal binding occurs directly on free species and also through the binding of sulfate complexes. Various functional groups such as amines (primary, secondary, and tertiary), hydroxyls, carboxyl groups, and phosphates may be active binding sites. The binding mechanism involves the ion exchange of metal cation with Ca^{2+} or H^+ on carboxylic groups from alginate. On the other hand, chelation mechanisms contribute through the electron pairs on the O, N, and P functional groups. Scheme 2 shows the suggested structure reporting active functional groups. These groups can interact with positively charged metal ions (free REE^{3+}) or complexes (i.e., sulfate complex: $REE(SO_4)^+$). Scheme 3 summarizes the tentative mechanisms involved in metal uptake.



Scheme 3. Tentative mechanisms for metal sorption.

3.2.5. Sorption Selectivity

The complexity of industrial effluents, which are characterized by the presence of numerous metal ions, makes it necessary to evaluate the impact of the presence of other base metals on the recovery of REEs. In order to evaluate the selectivity of the sorbent for REEs, the sorption of target metals from multi-component solutions was investigated at different pH values (Figure 8). The selectivity coefficient is defined as the ratio of distribution coefficients, $D_{\text{REE}}/D_{\text{metal}}$:

$$SC_{\text{Pr}/\text{metal}} = \frac{D_{\text{Pr}}}{D_{\text{metal}}} = \frac{q_{\text{eq}}^{\text{Pr}}/C_{\text{eq}}^{\text{Pr}}}{q_{\text{eq}}^{\text{metal}}/C_{\text{eq}}^{\text{metal}}} \quad (1)$$

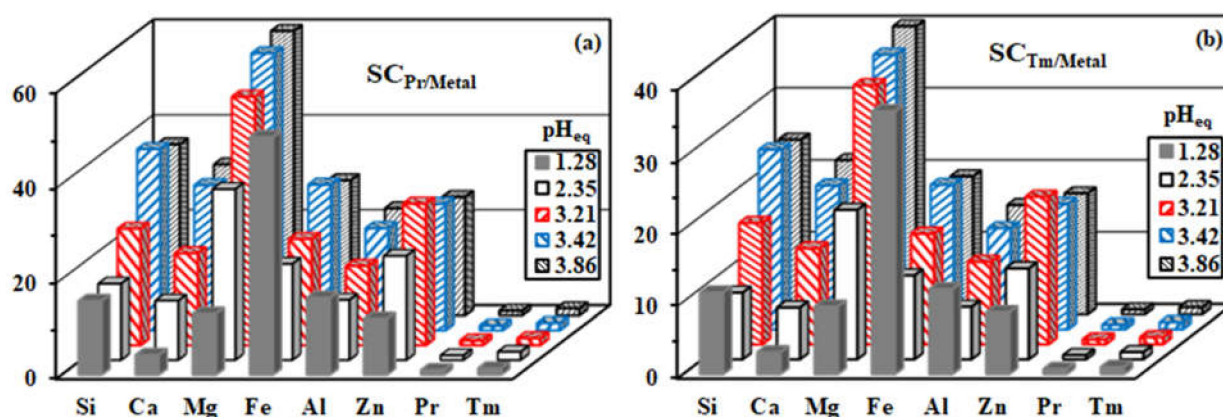


Figure 8. Effect of pH_{eq} on the selectivity coefficients of P2-APEI for Pr(III) (a) and Tm(III) (b) against other base metals and alkali-earth metals (equimolar 1 mM solutions; SD: 0.5 g L^{-1} ; contact time: 48 h; T: $22 \pm 1 \text{ }^\circ\text{C}$).

Figure 8 shows that P2-APEI has a strong selectivity for REEs against base metals (iron, aluminum, zinc), alkali-earth metals (calcium and magnesium), and metalloids (silicon). Consistent with previous studies in mono-component solutions, the sorption properties of Pr(III) and Tm(III) were so close that their separation with the sorbent was revealed to be difficult. The sorbent had little preference for Pr(III) vs. Tm(III): the $SC_{\text{Pr}/\text{Tm}}$ varied between 1.37 and 1.73 (depending on the pH); however, this preference is not sufficient for effectively achieving the separation of LREEs from HREEs.

Except for iron, the lowest selectivity coefficients of P2-APEI for REEs against competitor elements were observed at pH 1.28: $SC_{\text{Pr}/\text{Fe}}$ and $SC_{\text{Tm}/\text{Fe}}$ were close to 50 and 36, respectively. At the other pH values, the SC values generally increased with the pH. The sorbent also showed a higher selectivity against other metals for Pr(III) than for Tm(III). The best separation of REEs from other elements was reached for pH superior to 3.2 (except iron).

For Pr(III), the SC followed the series (SC, pH): $\text{Tm} \ll \text{Al}[2.5, \text{pH } 3.86] < \text{Zn}[29.7, \text{pH } 3.21] < \text{Ca}[31.7, \text{pH } 3.86] < \text{Si}[38.0, \text{pH } 3.42] \ll \text{Fe}[49.9, \text{pH } 1.28] \ll \text{Mg}[59.8, \text{pH } 3.86]$.

For Tm(III), the ranking followed: $\text{Pr} \ll \text{Al}[15.2, \text{pH } 3.86] < \text{Zn}[20.5, \text{pH } 3.21] < \text{Ca}[21.4, \text{pH } 3.86] < \text{Si}[24.9, \text{pH } 3.42] \ll \text{Fe}[36.5, \text{pH } 1.28] \ll \text{Mg}[40.3, \text{pH } 3.86]$.

The competition effect may be controlled by several parameters such as the ionic charge of the competitor metal, the ionic radius, and the hard/soft behavior. For trivalent cations, the sorbents had a lower selectivity against Al(III) than Fe(III), which are both considered hard acids. However, Al(III) had a smaller hydrated radius (i.e., 0.535 \AA) than Fe(III) (i.e., 0.645 \AA). In addition, the Fe(III) solution electronegativity was higher than that of Al(III) ($\chi = 3.835$ vs. 3.435); the softness parameter, σ , was $+0.33$ for Fe(III) vs. -0.31 for Al(III). In the case of divalent cations, Zn(II) ranked in the borderline class according to the HSAB theory, contrary to Mg(II) and Ca(II), which are hard acids. This ranking is not sufficient for explaining the specific behavior of Zn(II), for which the selectivity coefficient was comparable to Ca(II), but was much lower than Mg(II). Zn(II) had a hydrated radius

comparable to Mg(II) (0.72 Å vs. 0.74 Å) and was much lower than Ca(II) (i.e., 1.12 Å). Zn(II) had a positive softness σ (i.e., +0.35) contrary to Ca(II) and Mg(II) (i.e., −0.66 and −0.41, respectively). The solution electronegativity χ cannot be correlated to the selectivity order: 2.796 for Zn(II), 2.158 for Mg(II), and 1.862 for Ca(II). The different criteria showed contradictory trends regarding the evolution of the SC coefficient of REEs vs. these competitor cations. Therefore, it appears difficult to correlate the binding of the competitor ions with these physicochemical characteristics.

Figure S10 shows the \log_{10} plot of the distribution ratio of selected metals vs. the equilibrium pH. The quasi-linear curves shifted by one to two orders of magnitude for REEs compared with other competitor elements. In conclusion, despite the difficulty in interpreting the relative effects, at pH 3.2–3.9, P2-APEI showed a clear preference for REEs against other divalent or trivalent cations that are frequently present in the ore leachates.

Table S8 summarizes the semi-quantitative EDX analysis of the surface and cross-cut section for the P2-APEI sorbent after contact with multi-metal solutions at different pH values. The morphology of the material was not changed by the pH at both the surface and in the crosscut section. The semi-quantitative analysis confirmed the trends observed in the mass balance of individual metals during the sorption step (and the effect of pH in metal recovery). The concentrations of the REEs were of the same order of magnitude at the surface and in the inner part of the sorbent. This result confirms the readily accessibility of internal reactive groups for target metals.

3.2.6. Metal Desorption and Sorbent Recycling

Previous studies have shown the efficiency of acid solutions for the desorption of metal ions from functionalized APEI beads. The stability of the material can be improved by introducing calcium chloride (for the stabilization of alginate matrix). The metal-loaded sorbents collected at the end of the sorption process were tested for metal desorption using 0.2 M HCl/0.5 M CaCl₂ solutions for the study of the desorption kinetics (Figure 9 for mono-metal samples, Figure S11 for bi-metal samples). These curves clearly show that the desorption of both Pr(III) and Tm(III) was highly efficient for both APEI and P2-APEI: metal desorption systematically exceeded 99% and the time required for achieving these elution rates did not exceed 25–30 min. For mono-metal loaded resins, the desorption profiles were overlapped for the APEI sorbent, while for P2-APEI Pr(III), desorption was apparently faster than for Tm(III). In the case of sorbents loaded with binary solutions, the desorption profiles were also a little faster for Pr(III) compared with Tm(III). The PFORE and the PSORE equations were applied to fit the kinetic profiles [76].

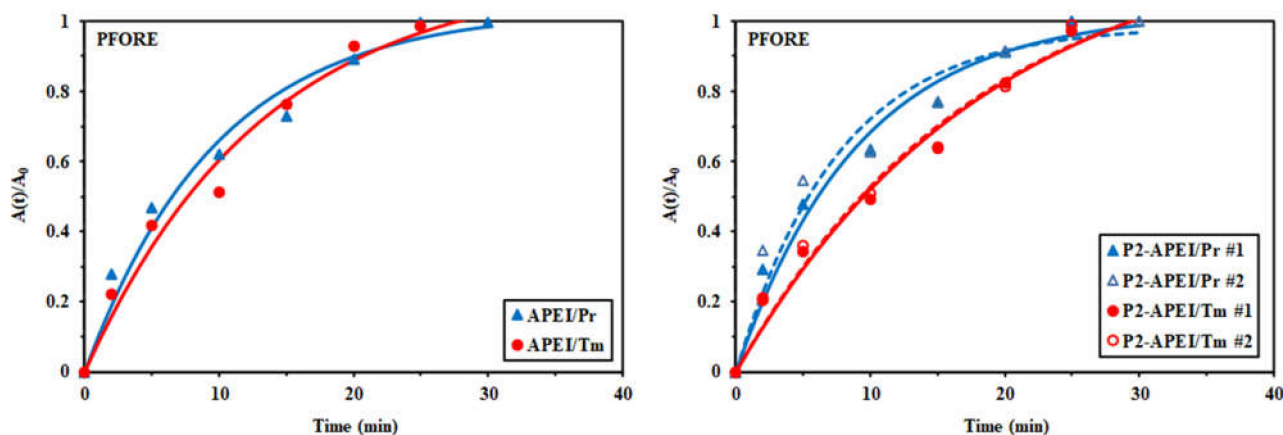


Figure 9. Pr(III) and Tm(III) desorption kinetics for APEI and P2-APEI—modeling with the PFORE (loaded sorbents collected from uptake kinetics; desorption using 0.2 M HCl/0.5 M CaCl₂; SD: 1 g L^{−1}, T: 22 ± 1 °C; A(t)/A₀: metal amount desorbed referred to initial sorbed amount).

Tables 6 and 7 report the parameters of these models for Pr(III) and Tm(III) desorption from APEI and P2-APEI loaded with mono-metal solutions; the data for bi-metal loaded sorbents are reported in Table S9. In most cases, the PSORE better fit the experimental profiles (especially for Pr(III) sorption), contrary to the sorption step that was preferentially described by the PFORE, probably due to the contribution of a ligand exchange mechanism. However, it is noteworthy that the PFORE allows for better approaching the effective sorption capacity, which is significantly overestimated by the PSORE, especially for Tm(III) recovery. The comparison of the orders of magnitude of the rate coefficients for desorption, both k_{d1} and k_{d2} , with the relevant values for the sorption step showed relatively faster desorption. On the other hand, the comparison of rate coefficients for binary solutions with mono-component solutions showed that desorption was faster for binary systems in the case of APEI sorbent, in contrast to P2-APEI (where the rate coefficients were higher for mono-component solutions).

Table 6. Pr(III) desorption kinetics using APEI and P2-APEI sorbents—fitting parameters for the PFORE and PSORE models.

Model	Parameter	Sorbent		
		APEI	P2-APEI	
			1st Run	2nd Run
Exp. PFORE	$q_{eq,exp}$ (mmol g ⁻¹)	0.0788	0.356	0.347
	$q_{1,calc}$ (mmol g ⁻¹)	0.0813	0.365	0.343
	$k_1 \times 10$ (min ⁻¹)	1.02	1.10	1.32
	R ²	0.980	0.983	0.962
	AIC	-82	-59	-53
PSORE	$q_{2,calc}$ (mmol g ⁻¹)	0.105	0.466	0.419
	$k_2 \times 10$ (L mmol ⁻¹ min ⁻¹)	9.45	2.34	3.51
	R ²	0.987	0.990	0.976
	AIC	-86	-64	-58

Table 7. Tm(III) desorption kinetics using the APEI and P2-APEI sorbents—fitting parameters for the PFORE and PSORE models.

Model	Parameter	Sorbent		
		APEI	P2-APEI	
			1st Run	2nd Run
Exp. PFORE	$q_{eq,exp}$ (mmol g ⁻¹)	0.0609	0.271	0.270
	$q_{1,calc}$ (mmol g ⁻¹)	0.0693	0.343	0.336
	$k_1 \times 10$ (min ⁻¹)	0.756	0.531	0.553
	R ²	0.983	0.987	0.985
	AIC	-87	-65	-64
PSORE	$q_{2,calc}$ (mmol g ⁻¹)	0.0964	0.506	0.489
	$k_2 \times 10^1$ (L mmol ⁻¹ min ⁻¹)	6.45	0.777	0.855
	R ²	0.984	0.987	0.986
	AIC	-88	-66	-65

The PFORE and PSORE models were applied for desorption (according to Daneshvar et al., [76])

$$\text{PFORE - Desorption : } q_d = q_{d,1} \left(1 - e^{-k_{d,1} \times t} \right)$$

$$\text{PSORE - Desorption : } q_d = \frac{q_{d,2}^2 \times k_{d,2} \times t}{1 + (k_{d,2} \times q_{d,2} \times t)}$$

In a second step, the recycling of the functionalized sorbent was investigated using a 0.2 M HCl/0.5 M CaCl₂ solution (operating a washing step between each sorption and desorption steps). The comparison of sorption and desorption efficiencies is summarized in Table 8. Sorption efficiency progressively decreased with recycling. However, at the fifth cycle, the loss was close to 10% for both Pr(III) and Tm(III). On the other hand, the elution of target metals was complete and remarkably stable for the five cycles. Figure 2 shows that the FTIR spectrum of P2-APEI submitted to five cycles of sorption and desorption hardly changed. This may explain the relative stability in the sorption performances. On the other hand, the comparison of Tables S2c and S7c showed that the concentrations of Ca and Cl at the surface and in the crosscut section of the functionalized sorbent increased after elution due to ion-exchange mechanisms associated with the composition of the eluent (i.e., HCl and CaCl₂ solutions).

Table 8. Sorption and desorption performances (efficiencies, %) for five successive cycles for Pr(III) and Tm(III) recovery using the P2-APEI sorbent.

Metal Ion	Cycle	Sorption		Desorption	
		SE (%)	St. Dev. (%)	DE (%)	St. Dev. (%)
Pr(III)	#1	99.1	0.3	100.0	0.3
	#2	97.7	0.6	100.5	0.5
	#3	96.5	0.6	100.1	0.1
	#4	94.2	0.1	100.1	0.0
	#5	91.0	1.5	100.0	0.2
Tm(III)	#1	91.9	0.6	99.9	0.1
	#2	89.6	0.6	100.5	0.5
	#3	87.2	0.5	100.2	0.6
	#4	84.5	0.9	100.4	0.1
	#5	82.7	0.6	99.7	0.2

3.3. Application to Metal Recovery from Acid Leaching of Tailing Material

3.3.1. Pre-Treatment of Leachates

The compositions of the ore and tailing are compared in Table S10. Although the conventional acid leaching recovered ~50% to 90% of valuable metals, the characterization of tailings clearly demonstrates that some strategic metals (such as U, Cu, and REEs) are still present in the mining residues at relatively high concentrations. Table S11 reports the composition of the leachates produced after pug leaching of ore tailings. Based on the huge concentrations of iron and aluminum, pre-treatments steps were operated to first remove iron with a precipitation step of the leachate at pH 4, followed by the precipitation of aluminum at pH 5. The results summarized in Table S11 confirm the progressive reduction of iron and aluminum (abatement reached while the concentrations of the other elements were marginally affected by the pre-treatments (the loss was less than 8% for Si, 4% for Ca, 8% for Mn, 10% for Ni, 4% for Cu, and 16% for Zn). In the case of REEs, the losses were close to 3.6% for Pr, 6.1% for Nd, and 7.4% for Tm; this was confirmed by the 2.7% total loss of REEs while using the global REE index. The precipitation steps were relatively selective and did not induce substantial loss of strategic elements. The major elements present in the pre-treated solutions were Ca(II) (i.e., 1833 mg Ca L⁻¹) and Cu(II) (i.e., ~183 mg Cu L⁻¹); other elements were systematically lower than 100 mg L⁻¹. The global REE index was close to 94.9 mg L⁻¹. This level of concentration is consistent with the range of concentrations where sorption processes may be used.

3.3.2. Metal Recovery from Pre-Treated Solutions

The sorption process was applied to pre-treated leachates at different pH_{eq} values (ranging between 1.38 and 3.91). The residual concentrations are also summarized in Table S11. It appears that the sorption process poorly affects the residual concentrations of

the base metals (and metalloid): the concentrations decreased by less than 13% even in the most favorable pH conditions, with the remarkable exception of the Zn(II) concentration, which decreased by 25.3% at pH_{eq} 3.91. On the other hand, the pre-treated leachate was almost exhausted in terms of REEs: the recoveries reached 94% for Nd(III), 93.5% for Pr(III), and almost 93.1% for Tm(III) (84.3% in terms of global REE index) at the highest pH (pH_0 : 5, pH_{eq} : 3.91). The distribution ratios (D) increased with the pH for the different metals (Table S12); however, this enhancement was especially important for REEs and the D values were remarkably higher at pH_{eq} 3.91 (values in the range $1.36\text{--}1.56 \times 10^4 \text{ L g}^{-1}$). These results clearly demonstrate that, despite the complexity of the solutions, the sorbent had a high affinity for REEs, with a high effect of concentration and limited impact of competitor metal ions. Table S13 shows the micrographs of surface and crosscut sections of P2-APEI after being in contact with the pre-treated leachates at different pH values. The sorption process and the pH did not significantly affect the morphology of the material. Table S14 reports the semi-quantitative analysis of the sorbent exposed to the pre-treated leachate at pH_0 5. The complete family of REEs (with the remarkable exception of Sc) was detected both at the surface and in the internal compartment of the sorbent. It is noteworthy that Sc was not identified in the series of REEs and associated elements (such as Y).

3.3.3. Rare Earth Elements (REEs) Separation and Precipitation as Oxalate Salts

After the sorption step, metal-loaded P2-APEI was eluted with 0.2 M HCl/0.5 M CaCl_2 . Table S15 reports the concentration of metal ions in the eluate from the sorbents loaded at different pH values. For base metals (and metalloid, Si(IV)), the concentrations on the sorbent were very low, but the desorption was very efficient: desorption efficiencies were systematically higher than 94% (not shown) for optimized sorption pH (i.e., pH_0 5 and pH_{eq} 3.91). In the case of REEs, despite higher amounts of sorbed metals, the elution yields were maintained higher than 96% (for Tm) and up to 99% (for Nd). Oxalic acid (at controlled pH) is a very efficient and selective precipitating agent for the recovery of rare earth elements [11,77–79]. The treatment of eluates with oxalic acid solution (15%, w/w) at pH 1 allows for quantitatively recovering REEs: the precipitation efficiency ranged between 98% and 98.5% (not shown). Table S16 summarizes the concentrations of selected metals in the residue (filtrate) of the oxalic acid precipitation step. It is noteworthy that the oxalic acid precipitation method requires a sufficient amount of REEs to be present for efficient precipitation; this is not the case with the sorbents loaded at low pH and this can explain the relative high residual REE concentration when the sorbent was loaded at pH_{eq} equal or lower than 3.91. The weak residual concentrations of the REEs after oxalic acid precipitation for the eluates produced in the desorption of the sorbent loaded at the highest pH values, confirmed the strong efficiency of this treatment for the selective recovery of REEs from eluates. The combination of this treatment with the appropriate selection of the pH of sorption (at pH_0 4–5), and the desorption using the CaCl_2/HCl eluate allows for highly efficient recovery and separation of REEs from complex solutions. On the other hand, the base metals (and Si) eluted from the sorbent were poorly precipitated (in the range 3–20%). Therefore, the precipitate of REEs oxalate was supposed to be relatively pure. Table S17 shows the semi-quantitative EDX analysis of the oxalate precipitate collected from the eluate of the sorbent loaded at pH_0 5 (pH_{eq} 3.91). Carbon and oxygen are associated with the oxalate ligand, and the presence of nitrogen and calcium mark the only significant impurities present in the precipitate. The use of the concentrated acidic solution of calcium chloride for the elution of the sorbent may explain the presence of Ca (at weight/atomic concentrations close to 1%). Usually, the REE oxalate precipitates are finally submitted to a calcination process for producing pure REE oxides [79]. Figure S12 compares the distribution of REEs in the sorbent and the oxalate precipitate (based on semi-empirical EDX analyses) to verify that the elution/precipitation process can contribute to enrich and separate the REEs. The enrichment factor (EF), defined here as the ratio of the percentage of the REE in the oxalate precipitate to its fraction onto the sorbent, did not follow any

clear trend (atomic number, ionic radius, etc.). There was no correlation between their enrichment factor and belonging to LREEs or HREEs.

EF ranking: La(EF:0.14) < Lu < Er < Ho < Ce < Pm < Yb < Tb < Tm < Tm < Dy(EF:0.93) < Pr(EF: 1.24) < Gd < Y < Sm < Nd < Eu(EF:7.8).

The mass balance on the distribution of selected elements in the different compartments of the sequential treatments is presented for the different pHs in Figure 10 (pH₀ 5 and pH_{eq} 3.91, the optimum condition for REE separation from other base metals and metalloid) and Figure S13 (for other pH values). Consistently with their specific treatments, Fe and Al were recovered (>90%) in the precipitates collected at pH 4 and pH 5, respectively. For Si, Ca, Mn, Ni, Cu, and Zn, most of the metal ions were recovered in the solutions issued from the sorption step (poorly sorbed): around 80–90% (only 63.4% in the case of Zn).

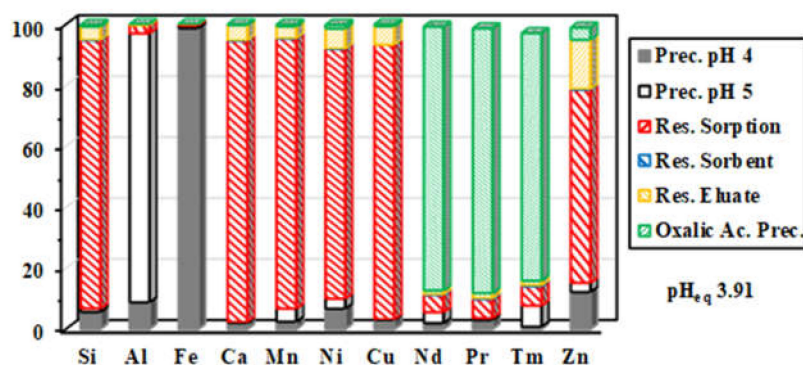


Figure 10. Distribution of the selected metals in the different compartments of the global treatment process (pH 4 precipitate (Fe); pH 5 precipitate (Al); residual solution after sorption at pH₀ 5 (Res. Sorption); metal residue on the sorbent after elution (Res. Sorbent), residue in the eluate and oxalic acid precipitate).

Low amounts of these elements were found in the residue of eluate precipitation (0–6.7%, 16.2% in the specific case of Zn). The rare earth elements were essentially collected in the oxalate precipitate: 86.9% for Pr, 86.6% for Nd, and 81.3% for Tm. The precipitation pre-treatments lost 3.5% (for Pr) to 7.6% (for Tm), the amounts of REEs not bound (released in the residue of sorption step) represented 5.7% to 6.3%, while the amounts tightly bound to the sorbent (not eluted) did not exceed 0.33%. The strong efficiency of oxalic precipitation for REE precipitation allows limiting their loss below 1.8%. For comparison, this distribution of metals in the different compartments for the other pH values (used for sorption step) is also reported in Figure S13: the other pH values induced less selective separation of the different metals.

4. Conclusions

A new member in the family of derivatives of alginate/algae biomass/PEI composites (APEI beads) was successfully synthesized by phosphorylation of the raw material. This functionalization was performed in two steps including the activation of the material with epichlorohydrin, followed by a reaction with triethyl phosphite. The combination of different analytical tools allowed for characterizing the physical (BET, TGA, SEM) and chemical (EDX, FTIR, XPS, titration) properties of the different materials. Successful functionalization was demonstrated, but these techniques also confirmed the contribution of different reactive groups (carboxylic, hydroxyl, amine, P-based groups) on the binding of a light REE (i.e., Pr(III)) and a heavy REE (i.e., Tm(III)) as free REE³⁺ or as a sulfate complex. The functionalization of APEI beads increased sorption performance by a factor close to 3. The sorption efficiency increased with the pH: optimum initial pH was found to be close to 5 (while the equilibrium pH tends to pH 4.3). The structure of the beads (macroporous scaffold) with a specific surface area close to 40 m² g⁻¹ may explain that the

resistance to intraparticle diffusion is negligible in the control of uptake kinetics, which are efficiently fitted by the pseudo-first order rate equation. Forty to 60 min was sufficient to reach equilibrium. The desorption of the REEs was also very efficient (higher than 98%) and fast (30–40 min) using 0.2 M HCl/0.5 M CaCl₂ solutions. The sorption and desorption performances were remarkably stable over five cycles: the loss in sorption efficiency was less than 10% at the fifth cycle, while the metal remained completely eluted even at the last cycle. Sorption isotherms were successfully modeled using the Langmuir equation and the maximum sorption capacities at the saturation of the monolayer were close to 2.14 mmol Pr g⁻¹ and 1.57 mmol Tm g⁻¹. These values were globally higher than those reported in the literature. Sorption tests performed in multi-metal solutions clearly demonstrate that the new sorbent had a marked preference for REEs against base metals or alkali-earth metals, especially at pH_{eq} 3.42–3.86. Although the selectivity was not high enough for separating Tm(III) from Pr(III), the sorbent had a preference for the lighter of the two REEs.

A process was designed for the valorization of tailing residues. The mining waste was the first pug leached to recover multi-metal solutions containing high concentrations of aluminum and iron, which are successively precipitated at pH 4 and pH 5 (with limited loss of other metal ions). In a second part of the process, the leachates were successfully treated by sorption for the recovery of REEs with relatively good separation from base metals, alkali earth elements, and Si(IV) by sorption on the phosphorylated sorbent. The desorption of the sorbent produced an eluate that contained most REEs and traces of zinc. The precipitation of the eluate with oxalic acid at pH 1 allows for selectively recovering REE-oxalate with good purity.

Supplementary Materials: The following are available online at <https://www.mdpi.com/2075-4701/11/2/294/s1>, Figure S1: title, Table S1: title, Video S1: title. Table S1a. Modeling of uptake kinetics, Table S1b. Modeling of sorption isotherms, Table S2a. SEM-EDX of raw beads (APEI)/surface and crosscut section, Table S2b. SEM-EDX analysis of activated chloride beads (spacer arm)/surface and crosscut section, Table S2c. SEM-EDX of sorbent after grafting of phosphoryl groups, Table S3. FTIR assignments and wavenumber (cm⁻¹) of APEI, APEI-Cl, and P2-APEI beads, Table S4. FTIR assignments and wavenumber (cm⁻¹) of P2-APEI, loaded sorbent with either Pr(III) and Tm(III), and after five cycles of sorption and desorption, Table S5a. C 1s signal for APEI and P2-APEI (before and after metal sorption), Table S5b. O 1s signal for APEI and P2-APEI (before and after metal sorption), Table S5c. N 1s signal for APEI and P2-APEI (before and after metal sorption), Table S5d. P 2p signal for APEI and P2-APEI (before and after metal sorption), Table S5e. XPS signals, assignments, and atomic fraction (AF into parenthesis) for APEI and P2-APEI (before and after metal sorption), Table S6. Elemental analysis of APEI and P2-APEI sorbents, Table S7a. SEM-EDX of raw beads (APEI) before and after loading with Pr(III) and Tm(III) (surface and crosscut section) at pH₀ 5, Table S7b. SEM-EDX of loaded P2-APEI sorbent (surface and crosscut section), Table S7c. SEM-EDX of P2-APEI sorbent after elution (surface and crosscut section), Table S8. SEM-EDX analysis of P2-APEI after being treated with an equimolar solution at different pH values, Table S9. Pr(III) and Tm(III) desorption kinetics using APEI and P2-APEI sorbents from binary solutions—fitting parameters for the PFORE and PSORE models, Table S10. Composition of ore and tailing—main elements, Table S11. Composition of tailing leachate and after successive pre-treatments, Table S12. Distribution ratio (D, L g⁻¹) for the sorption of metals from pre-treated leachates (at different values of pH_{eq}), Table S13. SEM analysis of P2-APEI beads (surface and crosscut section) after the sorption step onto the pre-treated leachate of tailings, Table S14. EDX analysis of the sorbent (surface and crosscut section) after application at pH₀ 5, Table S15. Metal concentrations (mg L⁻¹) in the eluate from sorbent loaded at different values of pH_{eq}, Table S16. Metal concentrations (mg L⁻¹) in the residue of oxalic acid precipitation from eluates collected from the sorbent loaded at different values of pH_{eq}, Table S17. EDX analysis of the oxalate precipitate from the sorbent loaded at pH₀ 5. Figure S1. Textural analysis of APEI and P2-APEI sorbents—(a) S_{BET} surface area, (b) pore size distribution, Figure S2. Thermogravimetric analysis of the APEI and P2-APEI sorbents, Figure S3. FTIR spectra of APEI, activated APEI (chloromethylated APEI, APEI-Cl), and phosphorylated APEI (P2-APEI) beads (focus on selected wavenumber ranges), Figure S4. FTIR spectra of sorbents (before and after metal sorption, and after regeneration) (focus on specific wavenumber ranges), Figure S5.

Determination of pH_{PZC} for APEI and P2-APEI sorbents, Figure S6. Pr(III) and Tm(III) speciation diagrams (experimental conditions used for the study of pH effect), Figure S7. pH variation during Pr(III) and Tm(III) sorption using APEI (a) and P2-APEI (b) sorbents, Figure S8a. Pr(III) and Tm(III) uptake kinetics using APEI and P2-APEI sorbents (duplicate experiments), Figure S8b. Pr(III) and Tm(III) uptake kinetics using APEI and P2-APEI sorbents from binary solutions, Figure S9. Pr(III) and Tm(III) sorption isotherms using APEI and P2(APEI (duplicate experiments), Figure S10. Effect of pH_{eq} on the distribution ratio of selected metals ($\log_{10} D$ plots), Figure S11. Pr(III) and Tm(III) desorption kinetics for APEI and P2-APEI from the binary solution—modeling with the PFORE, Figure S12. Relative percentages of the different REEs in the sorbent (cross-section) at pH_0 : 5, (a) and in the oxalic acid precipitate (b) (semi-quantitative EDX analysis), Figure S13. Distribution of selected metals in the different compartments of the global treatment process (pH 4 precipitate (Fe); pH 5 precipitate (Al); residual solution after sorption at different pH_0 values (Res. Sorption); metal residue on the sorbent after elution (Res. Sorbent), Residue in the eluate and the oxalic acid precipitate), Scheme S1. Proposed flow sheet for the treatment of ore residue.

Author Contributions: Methodology, experiment design and investigation: Y.W., E.G., H.M., and M.F.H.; Validation, characterization of sorbents and experiments: C.H., K.A.M.S., M.F.H., and K.Z.E.; Formal analysis, data curation, and visualization: K.A.M.S., H.M., A.A.-H.A.-R., and K.Z.E., software: C.H.; Data analysis, writing and editing: Y.W. and M.F.H.; Analyzed the data, writing, and editing; supervision: Y.W., M.F.H., and Y.W.; Funding acquisition: Y.W. All authors have read and agreed to the published version of the manuscript.

Funding: Y.W. thanks the support of the National Natural Science Foundation of China (NSFC) Projects (No. 11975082, U1967218); the Science and Technology Major Project of Guangxi Province (China) (AA17204100, AA18118030). E.G., M.F.H., A.A.-H.A.-R., and H.M. acknowledge the Institut Francais d’Egypte and Egyptian Academy of Science and Technology, Egypt for supporting the collaboration between IMT-Mines Ales and Nuclear Materials Authority through IMHOTEP project “MetalValor” (ref. 39529QA).

Data Availability Statement: The data presented in this study are available on request from the corresponding authors.

Conflicts of Interest: The authors declare no conflict of interest.

Abbreviations

PEI	Polyethyleneimine
APEI	Algal-polyethyleneimine
APEI-Cl	Methylene chloride grafted spacer arms (APEI-with epichlorohydrin)
P2-APEI	Phosphorylation of algal-polyethyleneimine
ICP-AES	Inductively coupled plasma atomic emission spectroscopy
FTIR	Fourier transform infrared spectroscopy
XPS	X-ray photoelectron spectroscopy
TGA	Thermal gravimetric analysis or thermogravimetric analysis
SEM	Scanning electron microscope
SEM-EDX	Scanning electron microscopy-energy dispersive x-ray analysis
BET	Brunauer-Emmett-Teller
DrDTG	Derivative-differential thermogravimetric analysis
SD	Sorbent dosage
PFORE	Pseudo-first order rate equation
PSORE	Pseudo-second order rate equation
RIDE	Resistance to intraparticle diffusion equation—Crank equation
AIC	Akaike information criterion
SC	selectivity coefficient
pH_{PZC}	Point of zero charge
pH_0	Initial pH of the solution
pH_{eq}	Equilibrium pH after sorption
K_d	Distribution ratio

C_0	Initial concentration
C_{eq}	Equilibrium concentration after metal sorption
BEs	Binding energies
AF	Atomic fractions
REEs	Rare earth elements
HSAB	Hard and Soft Acid-Base theory
Biopolymer-LDH	Biopolymer-layered double hydroxides composite

References

- Zhou, B.; Li, Z.; Chen, C. Global Potential of Rare Earth Resources and Rare Earth Demand from Clean Technologies. *Minerals* **2017**, *7*, 203. [[CrossRef](#)]
- Wall, F. Rare earth elements. In *Critical Metals Handbook*; Wiley: Hoboken, NJ, USA, 2014; pp. 312–339.
- Duarte, F.J. *Tunable Lasers Handbook*; Elsevier Academic Press: San Diego, CA, USA, 1995; 477p.
- Haxel, G.B.; Hedrick, J.B.; Orris, G.J.; Stauffer, P.H.; Hendley, J.W. *Rare Earth Elements: Critical Resources for High Technology*; Fact Sheet 087-02; U.S. Geological Survey: Reston, VA, USA, 2002. [[CrossRef](#)]
- RSC. Periodic Table. Available online: <https://www.rsc.org/periodic-table/> (accessed on 30 October 2020).
- Swain, N.; Mishra, S. A review on the recovery and separation of rare earths and transition metals from secondary resources. *J. Clean. Prod.* **2019**, *220*, 884–898. [[CrossRef](#)]
- Xu, D.; Shah, Z.; Cui, Y.; Jin, L.; Peng, X.; Zhang, H.; Sun, G. Recovery of rare earths from nitric acid leach solutions of phosphate ores using solvent extraction with a new amide extractant (TODGA). *Hydrometallurgy* **2018**, *180*, 132–138. [[CrossRef](#)]
- Yuan, H.; Hong, W.; Zhou, Y.; Pu, B.; Gong, A.; Xu, T.; Yang, Q.; Li, F.; Qiu, L.; Zhang, W.; et al. Extraction and back-extraction behaviors of 14 rare earth elements from sulfuric acid medium by TODGA. *J. Rare Earths* **2018**, *36*, 642–647. [[CrossRef](#)]
- Jia, Q.; Wang, Z.H.; Li, D.Q.; Niu, C.J. Adsorption of heavy rare earth(III) with extraction resin containing bis(2,4,4-trimethylpentyl) mono thiophosphinic acid. *J. Alloys Compd.* **2004**, *374*, 434–437. [[CrossRef](#)]
- Xiong, C.; Zhu, J.; Shen, C.; Chen, Q. Adsorption and Desorption of Praseodymium (III) from Aqueous Solution Using D72 Resin. *Chin. J. Chem. Eng.* **2012**, *20*, 823–830. [[CrossRef](#)]
- Yamada, E.; Murakami, H.; Nishihama, S.; Yoshizuka, K. Separation process of dysprosium and neodymium from waste neodymium magnet. *Sep. Purif. Technol.* **2018**, *192*, 62–68. [[CrossRef](#)]
- Omodara, L.; Pitkäaho, S.; Turpeinen, E.-M.; Saavalainen, P.; Oravisjärvi, K.; Keiski, R.L. Recycling and substitution of light rare earth elements, cerium, lanthanum, neodymium, and praseodymium from end-of-life applications—A review. *J. Clean. Prod.* **2019**, *236*, 117573. [[CrossRef](#)]
- Van der Hoogerstraete, T.; Binnemans, K. Highly efficient separation of rare earths from nickel and cobalt by solvent extraction with the ionic liquid trihexyl(tetradecyl)phosphonium nitrate: A process relevant to the recycling of rare earths from permanent magnets and nickel metal hydride batteries. *Green Chem.* **2014**, *16*, 1594–1606. [[CrossRef](#)]
- Zhao, F.; Repo, E.; Meng, Y.; Wang, X.; Yin, D.; Sillanpää, M. An EDTA-beta-cyclodextrin material for the adsorption of rare earth elements and its application in preconcentration of rare earth elements in seawater. *J. Coll. Interface Sci.* **2016**, *465*, 215–224. [[CrossRef](#)]
- Abreu, R.D.; Morais, C.A. Study on separation of heavy rare earth elements by solvent extraction with organophosphorus acids and amine reagents. *Miner. Eng.* **2014**, *61*, 82–87. [[CrossRef](#)]
- Huang, X.; Dong, J.; Wang, L.; Feng, Z.; Xue, Q.; Meng, X. Selective recovery of rare earth elements from ion-adsorption rare earth element ores by stepwise extraction with HEH(EHP) and HDEHP. *Green Chem.* **2017**, *19*, 1345–1352. [[CrossRef](#)]
- Sharaf, M.; Yoshida, W.; Kubota, F.; Goto, M. Selective Extraction of Scandium by a Long Alkyl Chain Carboxylic Acid/Organophosphonic Ester Binary Extractant. *Solvent Extr. Ion Exch.* **2018**, *36*, 647–657. [[CrossRef](#)]
- Singh, D.K.; Anitha, M.; Kain, V. Development of solvent extraction process for erbium purification. *Sep. Sci. Technol.* **2017**, *52*, 2284–2290. [[CrossRef](#)]
- Chen, J.; Luo, W.; Guo, A.; Luo, T.; Lin, C.; Li, H.; Jing, L. Preparation of a novel carboxylate-rich palygorskite as an adsorbent for Ce³⁺ from aqueous solution. *J. Coll. Interface Sci.* **2018**, *512*, 657–664. [[CrossRef](#)]
- Borai, E.H.; Hamed, M.G.; El-Kamash, A.M.; Siyam, T.; Elsayed, G.O. Template polymerization synthesis of hydrogel and silica composite for sorption of some rare earth elements. *J. Coll. Interface Sci.* **2015**, *456*, 228–240. [[CrossRef](#)] [[PubMed](#)]
- Florek, J.; Giret, S.; Juère, E.; Larivière, D.; Kleitz, F. Functionalization of mesoporous materials for lanthanide and actinide extraction. *Dalton Trans.* **2016**, *45*, 14832–14854. [[CrossRef](#)] [[PubMed](#)]
- Gargari, J.E.; Kalal, H.S.; Shakeri, A.; Khanchi, A. Synthesis and characterization of Silica/polyvinyl imidazole/H₂PO₄-core-shell nanoparticles as recyclable adsorbent for efficient scavenging of Sm(III) and Dy(III) from water. *J. Coll. Interface Sci.* **2017**, *505*, 745–755. [[CrossRef](#)] [[PubMed](#)]
- Ravi, S.; Lee, Y.-R.; Yu, K.; Ahn, J.-W.; Ahn, W.-S. Benzene triamido-tetraphosphonic acid immobilized on mesoporous silica for adsorption of Nd³⁺ ions in aqueous solution. *Microporous Mesoporous Mater.* **2018**, *258*, 62–71. [[CrossRef](#)]
- Maranescu, B.; Lupa, L.; Visa, A. Synthesis, characterization and rare earth elements adsorption properties of phosphonate metal organic frameworks. *Appl. Surf. Sci.* **2019**, *481*, 83–91. [[CrossRef](#)]

25. Saha, D.; Akkoyunlu, S.D.; Thorpe, R.; Hensley, D.K.; Chen, J. Adsorptive recovery of neodymium and dysprosium in phosphorous functionalized nanoporous carbon. *J. Environ. Chem. Eng.* **2017**, *5*, 4684–4692. [[CrossRef](#)]
26. Ang, K.L.; Li, D.; Nikoloski, A.N. The effectiveness of ion exchange resins in separating uranium and thorium from rare earth elements in acidic aqueous sulfate media. Part 2. Chelating resins. *Miner. Eng.* **2018**, *123*, 8–15. [[CrossRef](#)]
27. Fila, D.; Hubicki, Z.; Kołodyńska, D. Recovery of metals from waste nickel-metal hydride batteries using multifunctional Diphonix resin. *Adsorption* **2019**, *25*, 367–382. [[CrossRef](#)]
28. Gallhoun, A.A.; Elshehy, E.A.; Tolan, D.A.; El-Nahas, A.M.; Taketsugu, T.; Nishikiori, K.; Akashi, T.; Morshedy, A.S.; Guibal, E. Synthesis of polyaminophosphonic acid-functionalized poly(glycidyl methacrylate) for the efficient sorption of La(III) and Y(III). *Chem. Eng. J.* **2019**, *375*, 121932. [[CrossRef](#)]
29. Hérès, X.; Blet, V.; Di Natale, P.; Ouattou, A.; Mazouz, H.; Dhiba, D.; Cuer, F. Selective Extraction of Rare Earth Elements from Phosphoric Acid by Ion Exchange Resins. *Metals* **2018**, *8*, 682. [[CrossRef](#)]
30. Park, H.-J.; Tavlarides, L.L. Adsorption of Neodymium(III) from Aqueous Solutions Using a Phosphorus Functionalized Adsorbent. *Ind. Eng. Chem. Res.* **2010**, *49*, 12567–12575. [[CrossRef](#)]
31. Radhika, S.; Nagaraju, V.; Kumar, B.N.; Kantam, M.L.; Reddy, B.R. Solid-liquid extraction of Gd(III) and separation possibilities of rare earths from phosphoric acid solutions using Tulsion CH-93 and Tulsion CH-90 resins. *J. Rare Earths* **2012**, *30*, 1270–1275. [[CrossRef](#)]
32. Pinto, J.; Henriques, B.; Soares, J.; Costa, M.; Dias, M.; Fabre, E.; Lopes, C.B.; Vale, C.; Pinheiro-Torres, J.; Pereira, E. A green method based on living macroalgae for the removal of rare-earth elements from contaminated waters. *J. Environ. Manag.* **2020**, *263*, 110376. [[CrossRef](#)] [[PubMed](#)]
33. Ramasamy, D.L.; Porada, S.; Sillanpää, M. Marine algae: A promising resource for the selective recovery of scandium and rare earth elements from aqueous systems. *Chem. Eng. J.* **2019**, *371*, 759–768. [[CrossRef](#)]
34. Wang, F.; Zhao, J.; Li, W.; Zhou, H.; Yang, X.; Sui, N.; Liu, H. Preparation of Several Alginate Matrix Gel Beads and their Adsorption Properties Towards Rare Earths (III). *Waste Biomass Valorization* **2013**, *4*, 665–674. [[CrossRef](#)]
35. Song, D.; Park, S.-J.; Kang, H.W.; Bin Park, S.; Han, J.-I. Recovery of Lithium(I), Strontium(II), and Lanthanum(III) Using Ca–Alginate Beads. *J. Chem. Eng. Data* **2013**, *58*, 2455–2464. [[CrossRef](#)]
36. Wang, F.; Zhao, J.; Pan, F.; Zhou, H.; Yang, X.; Li, W.; Liu, H. Adsorption Properties toward Trivalent Rare Earths by Alginate Beads Doping with Silica. *Ind. Eng. Chem. Res.* **2013**, *52*, 3453–3461. [[CrossRef](#)]
37. Wang, F.C.; Zhao, J.M.; Wei, X.T.; Huo, F.; Li, W.S.; Hu, Q.Y.; Liu, H.Z. Adsorption of rare earths (III) by calcium alginate-poly glutamic acid hybrid gels. *J. Chem. Technol. Biotechnol.* **2014**, *89*, 969–977. [[CrossRef](#)]
38. Wu, D.; Zhang, L.; Wang, L.; Zhu, B.; Fan, L. Adsorption of lanthanum by magnetic alginate-chitosan gel beads. *J. Chem. Technol. Biotechnol.* **2011**, *86*, 345–352. [[CrossRef](#)]
39. Xu, S.; Wang, Z.; Gao, Y.; Zhang, S.; Wu, K. Adsorption of rare earths(III) using an efficient sodium alginate hydrogel cross-linked with poly-gamma-glutamate. *PLoS ONE* **2015**, *10*. [[CrossRef](#)]
40. Cataldo, S.; Gianguzza, A.; Merli, M.; Muratore, N.; Piazzese, D.; Liveri, M.L.T. Experimental and robust modeling approach for lead(II) uptake by alginate gel beads: Influence of the ionic strength and medium composition. *J. Coll. Interface Sci.* **2014**, *434*, 77–88. [[CrossRef](#)]
41. Wang, Y.; Feng, Y.; Zhang, X.-F.; Zhang, X.; Jiang, J.; Yao, J. Alginate-based attapulgite foams as efficient and recyclable adsorbents for the removal of heavy metals. *J. Coll. Interface Sci.* **2018**, *514*, 190–198. [[CrossRef](#)]
42. Guo, Z.; Li, Q.; Li, Z.; Liu, C.; Liu, X.; Liu, Y.; Dong, G.; Lan, T.; Wei, Y. Fabrication of efficient alginate composite beads embedded with N-doped carbon dots and their application for enhanced rare earth elements adsorption from aqueous solutions. *J. Coll. Interface Sci.* **2020**, *562*, 224–234. [[CrossRef](#)]
43. Wang, S.; Vincent, T.; Faur, C.; Rodriguez-Castellón, E.; Guibal, E. A new method for incorporating polyethyleneimine (PEI) in algal beads: High stability as sorbent for palladium recovery and supported catalyst for nitrophenol hydrogenation. *Mater. Chem. Phys.* **2019**, *221*, 144–155. [[CrossRef](#)]
44. Wei, Y.; Salih, K.A.M.; Lu, S.; Hamza, M.F.; Fujita, T.; Vincent, T.; Guibal, E. Amidoxime Functionalization of Algal/Polyethyleneimine Beads for the Sorption of Sr(II) from Aqueous Solutions. *Molecules* **2019**, *24*, 3893. [[CrossRef](#)] [[PubMed](#)]
45. Hamza, M.F.; Salih, K.A.M.; Abdel-Rahman, A.A.-H.; Zayed, Y.E.; Wei, Y.; Liang, J.; Guibal, E. Sulfonic-functionalized algal/PEI beads for scandium, cerium and holmium sorption from aqueous solutions (synthetic and industrial samples). *Chem. Eng. J.* **2021**, *403*, 126399. [[CrossRef](#)]
46. Hamza, M.F.; Wei, Y.; Guibal, E. Quaternization of algal/PEI beads (a new sorbent): Characterization and application to scandium recovery from aqueous solutions. *Chem. Eng. J.* **2020**, *383*, 123210. [[CrossRef](#)]
47. Lopez-Ramon, M.V.; Stoeckli, F.; Moreno-Castilla, C.; Carrasco-Marin, F. On the characterization of acidic and basic surface sites on carbons by various techniques. *Carbon* **1999**, *37*, 1215–1221. [[CrossRef](#)]
48. Nayak, A.K.; Pal, A. Development and validation of an adsorption kinetic model at solid-liquid interface using normalized Gudermannian function. *J. Mol. Liq.* **2019**, *276*, 67–77. [[CrossRef](#)]
49. Shapiro, L. *Rapid Analysis of Silicate, Carbonate, and Phosphate Rocks*; Report No. 1401; U.S. Geological Survey: Reston, VA, USA, 1975; Volume 76, pp. 3–88.
50. Marczenko, Z. *Separation and Spectrophotometric Determination of Elements*, 2nd ed.; Ellis Horwood: Chichester, UK, 1986; 678p.

51. Davies, W.; Gray, W. A rapid and specific titrimetric method for the precise determination of uranium using iron(II) sulphate as reductant. *Talanta* **1964**, *11*, 1203–1211. [[CrossRef](#)]
52. Nazir, R.; Gaan, S. Recent developments in P(O/S)–N containing flame retardants. *J. Appl. Polym. Sci.* **2020**, *137*, 27. [[CrossRef](#)]
53. Demadis, K.D.; Paspalaki, M.; Theodorou, J. Controlled Release of Bis(phosphonate) Pharmaceuticals from Cationic Biodegradable Polymeric Matrices. *Ind. Eng. Chem. Res.* **2011**, *50*, 5873–5876. [[CrossRef](#)]
54. Haug, A. Dissociation of alginate. *Acta Chem. Scand.* **1961**, *15*, 950–952. [[CrossRef](#)]
55. Li, J.-N.; Liu, L.; Fu, Y.; Guo, Q.-X. What are the pKa values of organophosphorus compounds? *Tetrahedron* **2006**, *62*, 4453–4462. [[CrossRef](#)]
56. Galhoum, A.A.; Eisa, W.H.; El-Sayed, I.E.-T.; Tolba, A.A.; Shalaby, Z.M.; Mohamady, S.I.; Muhammad, S.S.; Hussien, S.S.; Akashi, T.; Guibal, E. A new route for manufacturing poly(aminophosphonic)-functionalized poly(glycidyl methacrylate)-magnetic nanocomposite—Application to uranium sorption from ore leachate. *Environ. Pollut.* **2020**, *264*, 114797. [[CrossRef](#)]
57. Crank, J. *The Mathematics of Diffusion*, 2nd ed.; Oxford University Press: Oxford, UK, 1975; 414p.
58. Ho, Y.S.; McKay, G. Pseudo-second order model for sorption processes. *Process. Biochem.* **1999**, *34*, 451–465. [[CrossRef](#)]
59. Hubbe, M.A.; Azizian, S.; Douven, S. Implications of apparent pseudo-second-order adsorption kinetics onto cellulosic materials: A review. *BioResources* **2019**, *14*, 7582–7626. [[CrossRef](#)]
60. Persson, I. Hydrated metal ions in aqueous solution: How regular are their structures? *Pure Appl. Chem.* **2010**, *82*, 1901–1917. [[CrossRef](#)]
61. Marcus, Y. *Ion Properties*; Marcel Dekker, Inc.: New York, NY, USA, 1997; 259p.
62. Hamza, M.F.; Lu, S.M.; Salih, K.A.M.; Mira, H.; Dhmees, A.S.; Fujita, T.; Wei, Y.Z.; Vincent, T.; Guibal, E. As(V) sorption from aqueous solutions using quaternized algal/polyethyleneimine composite beads. *Sci. Total. Environ.* **2020**, *719*, 137396. [[CrossRef](#)] [[PubMed](#)]
63. Hamza, M.F.; Mubark, A.E.; Wei, Y.; Vincent, T.; Guibal, E. Quaternization of Composite Algal/PEI Beads for Enhanced Uranium Sorption—Application to Ore Acidic Leachate. *Gels* **2020**, *6*, 12. [[CrossRef](#)] [[PubMed](#)]
64. Pearson, R.G. Acids and bases. *Science* **1966**, *151*, 172–177. [[CrossRef](#)]
65. Iftekhhar, S.; Srivastava, V.; Ramasamy, D.L.; Naseer, W.A.; Sillanpää, M. A novel approach for synthesis of exfoliated biopolymeric-LDH hybrid nanocomposites via in-situ coprecipitation with gum Arabic: Application towards REEs recovery. *Chem. Eng. J.* **2018**, *347*, 398–406. [[CrossRef](#)]
66. Rhauderwiek, T.; Zhao, H.; Hirschle, P.; Döblinger, M.; Bueken, B.; Reinsch, H.; De Vos, D.; Wuttke, S.; Kolb, U.; Stock, N. Highly stable and porous porphyrin-based zirconium and hafnium phosphonates—Electron crystallography as an important tool for structure elucidation. *Chem. Sci.* **2018**, *9*, 5467–5478. [[CrossRef](#)] [[PubMed](#)]
67. Sum, J.Y.; Ahmad, A.L.; Ooi, B.S. Selective separation of heavy metal ions using amine-rich polyamide TFC membrane. *J. Ind. Eng. Chem.* **2019**, *76*, 277–287. [[CrossRef](#)]
68. Surls, J.P.; Choppin, G.R. Equilibrium Sorption of Lanthanides, Americium and Curium on Dowex-50 Resin. *J. Am. Chem. Soc.* **1957**, *79*, 855–859. [[CrossRef](#)]
69. Philip, L.; Iyengar, L.; Venkobachar, C. Biosorption of U, La, Pr, Nd, Eu and Dy by *Pseudomonas aeruginosa*. *J. Ind. Microbiol. Biotechnol.* **2000**, *25*, 1–7. [[CrossRef](#)]
70. Vijayaraghavan, K.; Jegan, J. Entrapment of brown seaweeds (*Turbinaria conoides* and *Sargassum wightii*) in polysulfone matrices for the removal of praseodymium ions from aqueous solutions. *J. Rare Earths* **2015**, *33*, 1196–1203. [[CrossRef](#)]
71. Varshini, J.S.; Das, D.; Das, N. Optimization of parameters for praseodymium(III) biosorption onto biowaste materials using response surface methodology: Equilibrium, kinetic and regeneration studies. *Ecol. Eng.* **2015**, *81*, 321–327. [[CrossRef](#)]
72. Wang, S.Y.; Hamza, M.F.; Vincent, T.; Faur, C.; Guibal, E. Praseodymium sorption on *Laminaria digitata* algal beads and foams. *J. Coll. Interface Sci.* **2017**, *504*, 780–789. [[CrossRef](#)]
73. Saeed, M.M.; Ahmed, M. Effect of Temperature on Kinetics and Adsorption Profile of Endothermic Chemisorption Process: –Tm(III)–PAN Loaded PUF System. *Sep. Sci. Technol.* **2006**, *41*, 705–722. [[CrossRef](#)]
74. Rangabhashiyam, S.; Vijayaraghavan, K. Biosorption of Tm(III) by free and polysulfone-immobilized *Turbinaria conoides* biomass. *J. Ind. Eng. Chem.* **2019**, *80*, 318–324.
75. Iftekhhar, S.; Srivastava, V.; Ben Hammouda, S.; Sillanpää, M. Fabrication of novel metal ion imprinted xanthan gum-layered double hydroxide nanocomposite for adsorption of rare earth elements. *Carbohydr. Polym.* **2018**, *194*, 274–284. [[CrossRef](#)]
76. Daneshvar, E.; Vazirzadeh, A.; Niazi, A.; Kousha, M.; Naushad, M.; Bhatnagar, A. Desorption of Methylene blue dye from brown macroalga: Effects of operating parameters, isotherm study and kinetic modeling. *J. Clean. Prod.* **2017**, *152*, 443–453. [[CrossRef](#)]
77. Jorjani, E.; Shahbazi, M. The production of rare earth elements group via tributyl phosphate extraction and precipitation stripping using oxalic acid. *Arab. J. Chem.* **2016**, *9*, S1532–S1539. [[CrossRef](#)]
78. Da Silva, R.G.; Morais, C.A.; Teixeira, L.V.; Oliveira, É.D. Selective Precipitation of High-Quality Rare Earth Oxalates or Carbonates from a Purified Sulfuric Liquor Containing Soluble Impurities. *Min. Met. Explor.* **2019**, *36*, 967–977. [[CrossRef](#)]
79. Tunsu, C.; Lapp, J.B.; Ekberg, C.; Retegan, T. Selective separation of yttrium and europium using Cyanex 572 for applications in fluorescent lamp waste processing. *Hydrometallurgy* **2016**, *166*, 98–106. [[CrossRef](#)]